Cell Reports

Resource

Mds1^{CreERT2}, an inducible Cre allele specific to adult-repopulating hematopoietic stem cells

Graphical abstract

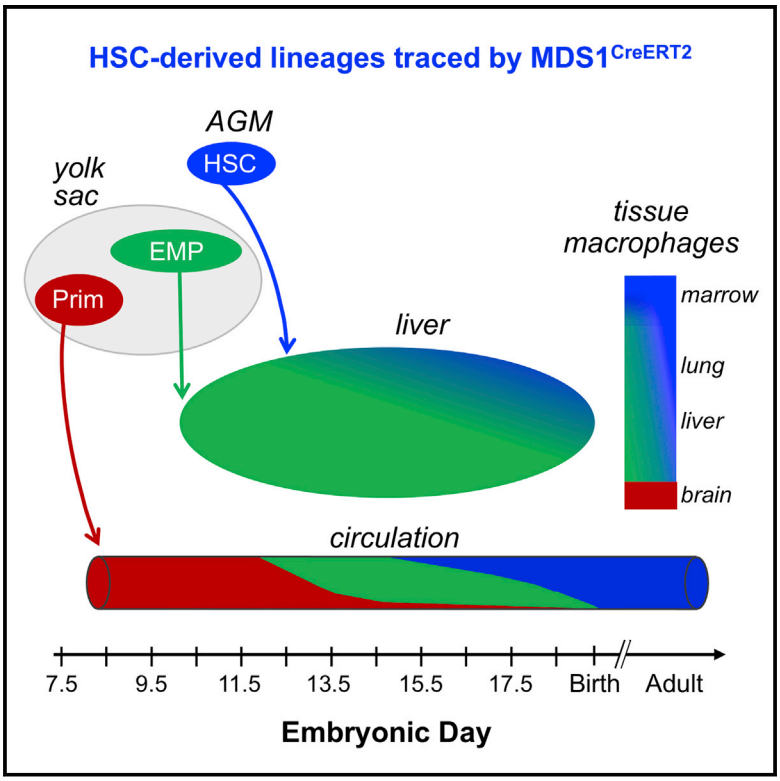

Highlights

- HSCs express *Mds1* as they emerge in the aorta of the murine fetus
- Inducible *Mds1*$^{Cre\text{-}ERT2}$ mice facilitate the lineage tracing of HSC-derived hematopoiesis
- HSC increasingly contribute to hematopoiesis in the fetal liver after E12.5
- The majority of macrophages in adult spleen and marrow are derived from HSCs

Authors

Yi Zhang, Kathleen E. McGrath, Edward Ayoub, ..., Sarah Rudzinskas, James Palis, Archibald S. Perkins

Correspondence

archibald_perkins@urmc.rochester.edu

In brief

Zhang et al. develop *Mds1*^{CreERT2} mice, which inducibly express Cre-recombinase in emerging fetal hematopoietic stem cells (HSCs). Lineage tracing reveals increasing HSC contributions to hematopoietic cells in E14.5–E16.5 embryos, as well as the majority of macrophages in adult spleen and marrow. *Mds1*^{CreERT2} mice will help deconvolute the complexity of hematopoietic ontogeny.

Zhang et al., 2021, Cell Reports *36*, 109562
August 17, 2021
https://doi.org/10.1016/j.celrep.2021.109562

CellPress

Cell Reports

CellPress
OPEN ACCESS

Resource

Mds1^{CreERT2}, an inducible Cre allele specific to adult-repopulating hematopoietic stem cells

Yi Zhang,[1,4] Kathleen E. McGrath,[2,4] Edward Ayoub,[1,3] Paul D. Kingsley,[2] Hongbo Yu,[1] Kate Fegan,[2] Kelly A. McGlynn,[1,3] Sarah Rudzinskas,[1] James Palis,[2,5] and Archibald S. Perkins[1,5,6,*]

[1]Department of Pathology and Laboratory Medicine, University of Rochester Medical Center, Rochester, NY 14642, USA
[2]Center for Pediatric Biomedical Research and Department of Pediatrics, University of Rochester Medical Center, Rochester, NY 14642, USA
[3]Department of Pharmacology and Physiology, University of Rochester Medical Center, Rochester, NY 14642, USA
[4]These authors contributed equally
[5]Senior author
[6]Lead contact
*Correspondence: archibald_perkins@urmc.rochester.edu
https://doi.org/10.1016/j.celrep.2021.109562

SUMMARY

Hematopoietic ontogeny consists of two broad programs: an initial hematopoietic stem cell (HSC)-independent program followed by HSC-dependent hematopoiesis that sequentially seed the fetal liver and generate blood cells. However, the transition from HSC-independent to HSC-derived hematopoiesis remains poorly characterized. To help resolve this question, we developed *Mds1*^{CreERT2} mice, which inducibly express Cre-recombinase in emerging HSCs in the aorta and label long-term adult HSCs, but not HSC-independent yolk-sac-derived primitive or definitive erythromyeloid (EMP) hematopoiesis. Our lineage-tracing studies indicate that HSC-derived erythroid, myeloid, and lymphoid progeny significantly expand in the liver and blood stream between E14.5 and E16.5. Additionally, we find that HSCs contribute the majority of F4/80+ macrophages in adult spleen and marrow, in contrast to their limited contribution to macrophage populations in brain, liver, and lungs. The *Mds1*^{CreERT2} mouse model will be useful to deconvolute the complexity of hematopoiesis as it unfolds in the embryo and functions postnatally.

INTRODUCTION

The emergence of the hematopoietic system during embryonic and fetal development has been the focus of extensive study, both for its paradigmatic value but also vis-à-vis its relevance to human diseases. Studies primarily in the murine model system indicate that the ontogeny of the hematopoietic system consists of two broad programs, an initial HSC-independent program followed by the emergence and establishment of an HSC-dependent program that arises from arterial vessels within the body of the embryo. HSC-independent hematopoiesis is complex, consisting of overlapping waves of primitive hematopoietic progenitors, erythro-myeloid progenitors (EMPs), and small numbers of lymphoid progenitors (Böiers et al., 2013; McGrath et al., 2015; Palis et al., 1999; Yoshimoto et al., 2011, 2012). Primitive hematopoiesis is derived from progenitors that emerge in the yolk sac beginning at embryonic day 7.25 (E7.25), producing circulating maturing primitive erythroid, megakaryocyte, and macrophage cells by E10 (Palis et al., 1999). Lineage-tracing experiments indicate that these first macrophages persist as adult self-renewing tissue-resident microglia (Hoeffel et al., 2015; Palis et al., 1999; Stremmel et al., 2018). Multilineage EMPs emerge from hemogenic endothelium in the yolk sac from E8.25 through E10.5 and seed the fetal liver as early as E10 to generate definitive erythroid, megakaryocyte, granulocyte, and monocyte lineage cells (Frame et al., 2016; Gomez Perdiguero et al., 2015; Lux et al., 2008; McGrath et al., 2015; Palis and Yoder, 2001). EMPs also provide tissue-resident macrophages that persist into adulthood in multiple organs including the liver, lungs, and skin (Gomez Perdiguero et al., 2015). Rare B cell and T cell progenitors arise independently of HSCs in the yolk sac and embryo proper by E9.5 (Yoshimoto et al., 2011, 2012), and lympho-myeloid-restricted progenitors (LMP) are already present in the fetal liver by E10.5, before HSC activity is detectable there (Boiers et al., 2013; Luis et al., 2016)

Small numbers of HSCs capable of long-term reconstitution of adult mouse recipients begin to emerge at E10.5 from the ventral aspect of the dorsal aorta (Yokomizo and Dzierzak, 2010). At E11.5–12.0, HSCs are found in the fetal liver where they subsequently expand in numbers (Ema and Nakauchi, 2000; Kumaravelu et al., 2002). However, the transition from HSC-independent to HSC-derived hematopoiesis in the murine fetus remains poorly characterized, particularly since the maturing erythroid, megakaryocytic, and myeloid progenies of EMPs and HSCs are not currently easily distinguishable. Several different inducible lineage-tracing approaches have been used to distinguish HSC-independent versus HSC-derived contributions based on promoters active both in HSCs and in HSC-independent progenitors, including (Cdh5 (Zovein et al., 2008), CSF1R-Cre (Qian et al., 2011), Kit-Cre (Stremmel et al., 2018), Runx1-Cre

(Samokhvalov et al., 2007), Tie2-Cre (Gomez Perdiguero et al., 2015), and TLR2-Cre (Balounová et al., 2019). The efficacy of these CreER alleles relies on the timing of induction during the staggered emergence of HSC-independent progenitors and of HSCs. However, the significant temporal overlap in the emergence of HSC-independent progenitors and of HSCs, coupled with the broad cellular expression of these promoters, and the imprecision of *in vivo* CreER induction often results both in incomplete and in mixed labeling (Gentek et al., 2018; Gomez Perdiguero et al., 2015; Hoeffel et al., 2015; Soares-da-Silva et al., 2021). An alternative approach is to specifically label emerging HSCs. Studies of emerging HSCs have identified several genes preferentially or specifically expressed in HSCs, including *Hlf* (Yokomizo et al., 2019), *Ly6A* (Sca-1; (Ma et al., 2002), *Procr* (Iwasaki et al., 2010), and *Mecom* (Yuasa et al., 2005).

The *Mecom* or *Mds1-Evi1 complex* locus was first identified as a site of proviral insertion in murine myeloid leukemias (Morishita et al., 1988; Mucenski et al., 1988) and was also found to be activated via chromosomal rearrangements in human AML (Bitter et al., 1985; Rubin et al., 1990). Importantly, the *Mds1-Evi1* gene harbors two widely separated transcription start sites (TSSs) (Fears et al., 1996) that encode a series of different isoforms, with the upstream TSS encoding MDS1-EVI1, a 160 kDa isoform harboring an N-terminal PR domain, thus placing this isoform in the PR/SET family of transcriptional regulators and chromatin modifiers (Hohenauer and Moore, 2012). The downstream TSS encodes at least three zinc finger protein isoforms of EVI1 (135/145, 123, and 103 kDa). Roles for *Mecom* in HSCs during embryogenesis have been documented by several groups. In the mouse, homozygous loss of all but the 103 kDa isoform results in loss of competitive repopulating ability within the para-aortic splanchnopleura and lethality by E10.5 (Hoyt et al., 1997; Yuasa et al., 2005). Knockout of all isoforms is associated with HSCs in the fetal liver that lack competitive repopulation ability and with lethality at E13.5 (Goyama et al., 2008). In contrast, the elimination of the 160 kDa MDS1-EVI1 isoform results in viable mice with diminished numbers of adult HSCs (Zhang et al., 2011) and with skeletal defects (Juneja et al., 2014). Using a zebrafish model, Konantz et al. (2016) documented expression of *Evi1* in the ventral aspect of the dorsal aorta, and downregulation of *Evi1* led to impaired HSC emergence from hemogenic endothelium.

To more clearly define the role of the different *Mecom* isoforms in the mammalian hematopoietic system, we introduced a *lacZ* reporter into the upstream TSS of murine *Mecom* ($Mds1^{lacZ}$) facilitating the examination of its expression histologically within the murine embryo. $Mds1^{lacZ}$ is expressed in $Runx1^{+}$ clusters in the ventral aspect of the dorsal aorta of the mouse but is not expressed in the fetal liver (Zhang et al., 2011). To probe this further, we developed a *Cre-ER* knockin into the *Mds1* locus ($Mds1^{CreERT2}$). Lineage-tracing studies using this mouse model revealed that the progeny of *Mds1*-expressing cells are subsequently found in the fetal liver as immunophenotypic and functional LT-HSCs. In contrast, neither EMPs themselves nor their progeny were labeled, nor were the progeny of primitive hematopoietic progenitors. Lineage tracing with $Mds1^{CreERT2}$ demonstrated that HSC-derived hematopoietic progeny are found in increasing numbers in the livers of E14.5 to E16.5 murine embryos and contribute significantly to circulating erythroid, myeloid, and lymphoid cells by E16.5. In addition, while varying degrees of tissue-resident macrophages in the brain, liver, and lung of adult mice originate from HSC-independent sources, the large majority of $F4/80^{+}$ macrophages in the spleen and bone marrow of adult mice are lineage labeled, consistent with their derivation from HSCs. The $Mds1^{CreERT2}$ model will be useful to address multiple questions regarding the complexity of the hematopoietic system as it unfolds in the murine embryo and continues to function postnatally.

RESULTS

Embryonic expression of Mecom

We reported previously the expression pattern of *Mecom* transcripts during embryogenesis using *in situ* hybridization probes that hybridized to both *Evi1* and *Mds1* transcripts. These studies revealed *Mds1-Evi1* transcripts in the developing limb bud, lung epithelium, and developing renal system among other locations, with no discernable expression in the fetal liver (Perkins et al., 1991). In an effort to understand more precisely where *Mds1* is expressed in the embryonic hematopoietic system, we created a nuclear localized *NLS-lacZ* knockin allele that puts the *lacZ* gene under transcriptional control of the *Mecom* upstream promoter (termed *Mds1*) (Fears et al., 1996; Zhang et al., 2011). Using this allele, termed $Mds1^{lacZ}$ (referred to as $Mds1^{m1}$ in Zhang et al., 2011), we conducted whole-mount labeling of E8.5 to E14.5 embryos with 5-bromo-4-chloro-3-indolyl-β-D-galactopyranoside (X-gal). β-galactosidase staining was evident in the limb buds, mesonephros, and vertebral bodies (Figures 1A–1E), overlapping considerably with the expression of *Mds1-Evi1* described previously by *in situ* hybridization (Perkins et al., 1991).

Coronal sections of E9.5, E10.5, and E11.5 embryos (Figures 1F–1H; Figures S1A and S1C) revealed LacZ staining of endothelial cells on the ventral aspect of the dorsal aorta, as well as in intra-aortic hematopoietic clusters (IAHC). Importantly, these LacZ-positive aortic endothelial cells were found to co-express Runx1, consistent with a hemogenic endothelial identity (Figure 1I; Figures S1B and S1D) (Yzaguirre et al., 2017). Given that HSCs are known to seed and expand within the fetal liver, we expected to detect β-galactosidase-staining cells in the fetal liver. Paradoxically, we did not find evidence of *Mds1-Evi1* expression in the fetal liver (Figure 1J), consistent with previous findings (Perkins et al., 1991). These data suggest that the expression of *Mds1-Evi1* in the fetal hematopoietic system is remarkably transient, in contrast to the expression of *Mds1-Evi1* in adult LT- and ST-HSCs (Zhang et al., 2011).

Generation of a mouse model of TAM-inducible Cre recombinase knocked into the Mds1 locus

To assess whether the β-gal-positive cells identified at E9.5 in the dorsal aorta of $Mds1^{lacZ}$ mice represent functional hematopoietic cells, we performed lineage-tracing experiments. We constructed an $Mds1^{CreERT2}$ allele in which a tamoxifen (TAM)-inducible Cre recombinase was inserted into the *Mecom*

CellPress
OPEN ACCESS

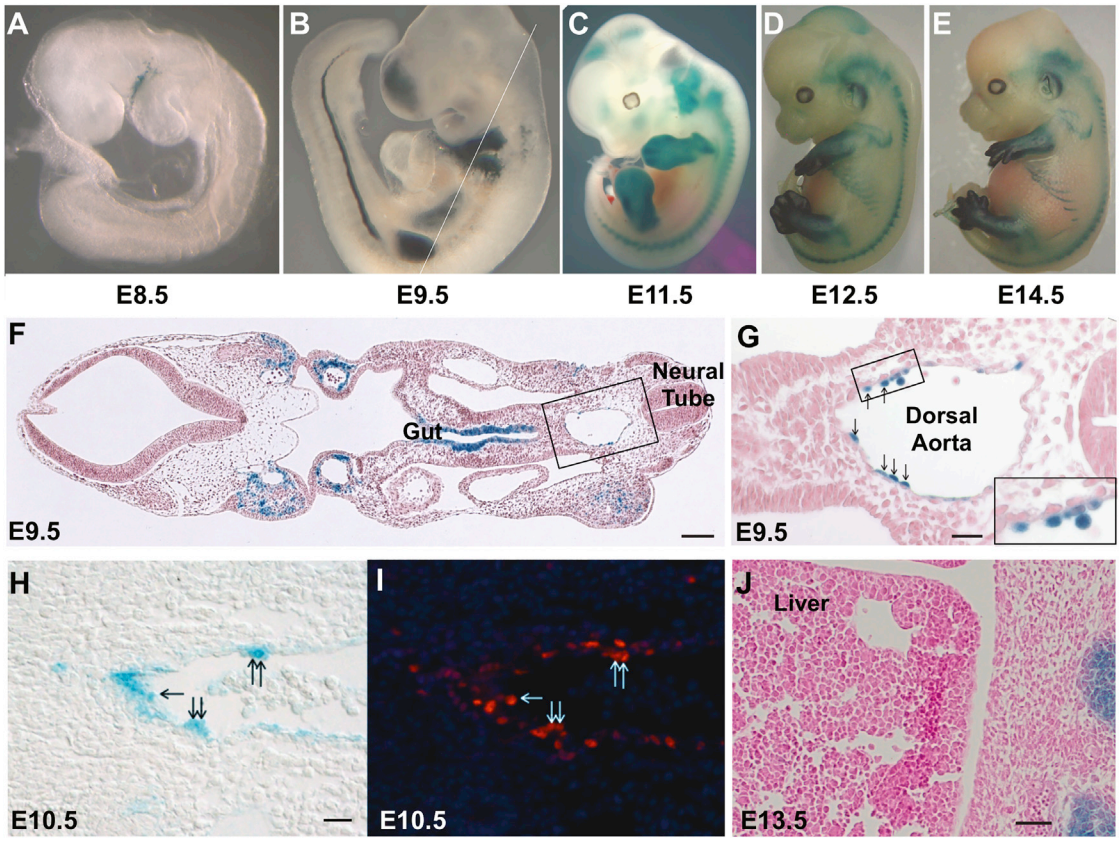

Figure 1. *Mds1* is expressed in aortic hemogenic endothelium

Embryo-fetal expression of *Mds1* documented using the $Mds1^{lacZ}$ allele (Zhang et al., 2011).

(A–E) Whole-mount β-galactosidase staining of heterozygous $Mds1^{lacZ/wt}$ embryos at various stages of development as indicated. Mean crown-rump length for C57 E8.5 = 1.88, E9.5 = 3.47, E11.5 = 6.83, E12.5 = 8.60, E14.5 = 12.29 mm (Mu et al., 2008).

(F) Photomicrograph of a X-gal-stained section of an E9.5 embryo with plane of section indicated by the white line in (B). Scale bar, 100 μM.

(G) Close-up of boxed region in (F), showing the dorsal aorta, left being ventral, right being dorsal, with β-galactosidase-positive cells seen budding from the endothelium (arrows). Scale bar, 25 μM.

(H and I) Photomicrographs of E10.5 aorta (left is ventral) β-galactosidase-positive cells (H) that also express Runx1 detected by immunocytochemistry (I). Scale bar, 20 μM.

(J) X-gal staining reveals no β-galactosidase-positive cells in the liver of the E13.5 mouse embryo. Scale bar, 25 μM.

locus so it would be expressed by the upstream TSS (Figures 2A and 2B). We first performed lineage tracing with the $Mds1^{CreERT2}$ allele in adult mice by combining it with the ubiquitously transcribed, Cre-dependent $Rosa26^{loxP\text{-}STOP\text{-}loxP\text{-}YFP}$ ($Rosa26^{LSL\text{-}YFP}$) reporter. Based on the restricted expression of *Mds1-Evi1* to adult LT- and ST-HSCs, as well as a small percentage of MPPs (Christodoulou et al., 2020; Zhang et al., 2011), we expected that activation of $Mds1^{CreERT2}$ via TAM treatment would result in increasing and broad YFP positivity in hematopoietic cells over time. $Mds1^{CreERT2}$ $Rosa26^{LSL\text{-}YFP}$ mice received five treatments of TAM over 5 days (Figure 2C). Analysis of bone marrow at 4, 10, and 15 days (relative to the first treatment) revealed a time-dependent increase in YFP^+ cells (Figure 2D). By 15 days, up to 40% of marrow cells were YFP^+ and they consisted of myeloid, erythroid, and lymphoid cells (data not shown). These labeled cells in the marrow contributed to YFP^+ progeny detected in the peripheral blood at 30 days (Figure 2E).

Lineage-tracing preHSCs and fetal liver cells with $Mds1^{CreERT2}$

To test whether the $Mds1^{lacZ}$-expressing cells present in the dorsal aorta might contain precursors of fetal liver hematopoiesis, we conducted lineage-tracing studies using the $Mds1^{CreERT2}$ allele crossed with a $Rosa26^{LSL\text{-}lacZ}$ reporter. Timed pregnant mice were treated with a single dose of TAM either at E7.5 or at E9.5, and embryos were harvested and stained for β-gal at E13.5. Labeling at E9.5 with TAM lineage traced small numbers of β-gal-positive cells in the fetal liver at E13.5, which were not seen when TAM was delivered at E7.5 (Figures 2F and 2G). While fetal liver cells themselves do not express *Mds1*, the fetal liver contains a population of cells derived from earlier *Mds1*-expressing cells.

We next investigated the specificity of the $Mds1^{CreERT2}$ lineage-tracing mouse model by analyzing E11.5 fetuses. Pregnant $Mds1^{CreERT2/wt}$ $Rosa26^{LSL\text{-}YFP/LSL\text{-}YFP}$ mice were treated with TAM at E9.5 and cells from aorta-gonad-mesonephros (AGM), yolk sac, blood, and liver in $Mds1^{CreERT2/wt}$ $Rosa26^{LSL\text{-}YFP/wt}$

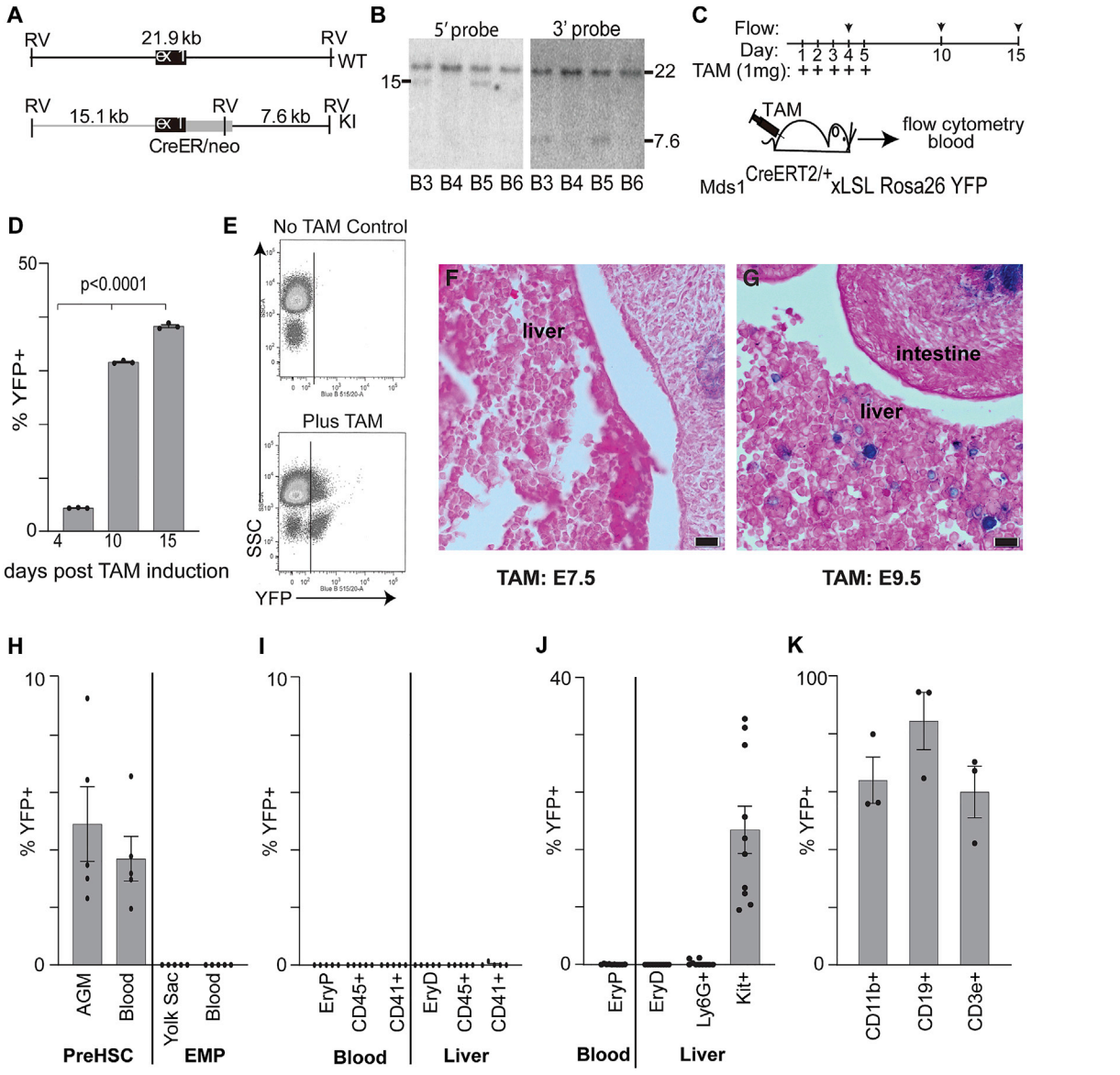

Figure 2. Tamoxifen-inducible *Mds1*^{CreERT2} allele construction and expression in adult hematopoiesis and fetal HSC but not EMP- or primitive-derived hematopoiesis

(A) A DNA cassette encoding the TAM-inducible Cre-ER fusion protein was introduced into the *Mecom* locus in embryonic stem (ES) cells via homologous recombination.

(B) ES cell DNA was screened by Southern blotting, cutting the genomic DNA with EcoRV and blotting with 5′ and 3′ probes situated outside of the recombination cassette. Clones B3 and B5 show the expected sizes of 15.1 Kb and 7.6 kb, with 5′ and 3′ probes, respectively. Mice were created from ES cell clone B5, which were backcrossed onto a C57Bl6 background and crossed with mice bearing the Rosa26 LSL-YFP allele.

(C–E) These mice were treated with TAM, and the peripheral blood was analyzed by flow cytometry at 30 days and bone marrow at days 4, 10, and 15 for YFP$^+$ cells, which progressively increased. (D) Quantitation of percentage of bone-marrow YFP-positive cells following the first TAM treatment on the days indicated. Average ± SEM, n = 3. (E) Representative scatterplot (day 30) showing the appearance of YFP$^+$ blood cells following TAM treatment.

(F and G) X-gal staining of fetal liver in E13.5 mouse embryos, after a single treatment with TAM at E7.5 (F) or E9.5 (G). Eosin counter-stain; bar denotes 10 μm.

(H) Flow cytometric analysis of E11.5 AGM, yolk sac, and blood for pre-HSC (kit$^+$CD31$^+$VECadherin$^+$) versus EMP (kit$^+$CD41$^+$CD16/32$^+$) as indicated. For each analysis, the percentage of total cells that were YFP$^+$ is charted as average ± SEM, n = 5. See Figures S2A and S2B, for the gating strategy.

(I) Flow cytometric analysis of E11.5 blood and liver for lineage-positive cell subsets (EryP Ter119$^+$ blood, EryD Ter119$^+$FSC^{hi} to distinguish from circulating EryP in the liver) as indicated. For each analysis, the percentage of total cells that were YFP$^+$ is charted as average ± SEM, n = 5. See Figures S2D and S2E for the gating strategy.

(legend continued on next page)

(referred to as *Mds1*^{CreERT2} *Rosa26*$^{LSL\text{-}YFP}$) fetuses were analyzed by flow cytometry. Cells from littermate negative control *Mds1*$^{WT/WT}$ *Rosa26*$^{LSL\text{-}YFP/wt}$ mice were used to determine bone fide YFP$^+$ expression in all experiments (data not shown). Consistent with the staining seen with *Mds1*^{lacz}, we found YFP$^+$CD31$^+$kit$^+$VE-cadherin$^+$ pre-HSCs ((Azzoni et al., 2018; Gao et al., 2020; Yokomizo and Dzierzak, 2010) in the AGM and in the circulation. In contrast, we found no labeling of CD41$^+$kit$^+$CD16/32$^+$ EMPs in the yolk sac, Ter119$^+$ primitive erythroid cells (EryP) in the bloodstream(Kingsley et al., 2004), or EMP-derived definitive erythroid cells (EryD) in the liver (McGrath et al., 2015; Gomez Perdiguero et al., 2015) (Figures 2H and 2I; Figures S2A and S2B). Other HSC-independent CD45$^+$ early myeloid cells and CD41$^+$ megakaryocytes in the bloodstream and in the liver were also not labeled (Figure 2I). The *Mds1*^{CreERT2} promoter did not label HSC-independent hematopoietic cells in E11.5 fetuses even when activated at E8.5 (Figure S2C). TAM treatment at E8.5 also did not label pre-HSCs, despite labeling a subset of cells in the paw, consistent with *Mds1* expression in limb buds (Figure S2C; Figure 1).

We next asked whether the *Mds1*^{CreERT2} can label functional HSC in the murine embryo. As E12.5 is the first time that a significant number of transplantable HSCs are found in the liver (Ema and Nakauchi, 2000; Kumaravelu et al., 2002), pregnant *Mds1*^{CreERT2} *Rosa26*$^{LSL\text{-}YFP}$ mice were treated with TAM at E9.5, and blood and liver were analyzed at E12.5. As seen at E11.5, primitive erythroid cells in the blood stream and definitive erythroid and granulocyte progeny of EMPs in the liver were not labeled (Figure 2J; Figures S2D and S2E). In contrast, YFP$^+$ cells in the E12.5 liver were found to constitute a subset of Kit$^+$ cells, suggesting that *Mds1*^{CreERT2} might be lineage-labeling HSCs. To directly test this hypothesis, we transplanted 2 × 10^6 E12.5 *Mds1*^{CreERT2} *Rosa26*$^{LSL\text{-}YFP}$ liver cells (induced with TAM at E9.5) into irradiated syngeneic recipient mice along with 2 × 10^5 wild-type bone-marrow cells. At 12 weeks post-transplant, peripheral blood from these recipients revealed a high percentage of YFP$^+$ T cells, B cells, and myeloid cells (Figure 2K; Figure S2F). Taken together, these data demonstrate that *Mds1*^{CreERT2}, combined with TAM induction at E9.5, lineage-traces fetal HSCs but not primitive erythropoiesis or EMP-derived hematopoiesis.

Mds1^{CreERT2} lineage tracing of later fetal hematopoiesis

We utilized the *Mds1*^{CreERT2} lineage-tracing mouse model to examine the transition from HSC-independent to HSC-derived hematopoiesis in livers of E14.5 and E16.5 mouse embryos (Figure 3). The level of labeling of HSC-enriched LSK (lineage$^-$, Sca1$^+$, Kit$^+$) cells was used to normalize for different efficiencies of excision. In contrast to E12.5 livers, YFP$^+$ Ter119$^+$ (definitive erythroid), Ly6G$^+$ (granulocyte), Ly6C$^+$ (monocyte), and CD19$^+$ (lymphoid) cells were readily evident at E14.5. This suggests that HSCs have begun to contribute to multiple hematopoietic lineages by E14.5 (Figure 3A; Figures S3A and S3B). Furthermore, at E14.5, the higher contribution of *Mds1*^{CreERT2}-labeled cells to the hematopoietic progenitor (LK, Lineage$^-$, Sca1$^-$, Kit$^+$) compartment compared to the downstream lineage-positive cells suggests that HSC contribution to fetal hematopoiesis is expanding (Figure 3A). Indeed, this is evident at E16.5, with the increased contribution of HSCs to the LK hematopoietic progenitor pool, as well as downstream to maturing erythroid-, granulocyte-, and monocyte-lineage cells (Figure 3B, left panel). Consistent with the progressive contribution of HSCs to fetal hematopoiesis, labeled myeloid cells and red blood cells are now also found in the bloodstream (Figure 3B, right panel, Figure S3C). Since the *Rosa26* locus is progressively downregulated in maturing erythroid cells (Asari et al., 2004; Zambrowicz et al., 1997), the YFP$^+$ fraction of circulating erythrocytes may underrepresent the full contribution from HSCs. Further analysis of E16.5 hematopoietic stem and progenitor cells indicated that fetal HSCs contribute equally to all lineage-biased MPP subsets, and to a lesser, but uniform degree to lineage-committed lymphoid (CD127$^+$), myeloid (CD16/32$^+$), and erythroid/megakaryocyte (CD16/32$^-$) progenitors (Figure 3C; Figure S3D; Pronk et al., 2007). Taken together, these data indicate that HSCs provide an increasing contribution to hematopoiesis in the fetal liver between E14.5 and E16.5, the time points associated with significant expansion of HSC numbers and differentiating hematopoietic progenitors and precursors in the fetal liver (Ema and Nakauchi, 2000; Kumaravelu et al., 2002)

Several tissue-resident macrophage populations, established from HSC-independent sources, persist through embryogenesis as self-renewing populations (Gomez Perdiguero et al., 2015; Hoeffel et al., 2015; Liu et al., 2019). This is particularly evident for microglia, which are seeded early in development and not normally replaced by later fetal or adult myeloid cells (Gomez Perdiguero et al., 2015; Hoeffel et al., 2015). Consistent with these findings, no YFP labeling of F4/80$^+$ macrophage cells in the E14.5 or 16.5 brain was evident in *Mds1*^{CreERT2} fetuses (Figure 3D; Figure S3E). In contrast, a high proportion of macrophages in the fetal liver are HSC-derived by E16.5 consistent with contribution of HSCs to the monocyte lineage (Figures 3B and 3D).

Lineage tracing of hematopoiesis in adult mice

TAM administration at E9.5 clearly activated Cre-ER in fetal cells capable of long-term engraftment when transplanted into adult recipients (Figure 2K). However, differences in the regulation of Flt3 in subsets of fetal HSCs has indicated that there is heterogeneity in fetal transplantable HSCs, including subsets that may not normally contribute to adult HSCs (Beaudin et al., 2016). To directly test whether precursors of adult HSCs were being labeled in the *Mds1*^{CreERT2} mouse model, E9.5 TAM-treated pregnancies containing *Mds1*^{CreERT2} *Rosa*$^{LSL\text{-}YFP}$ fetuses were allowed to come to term. After 1 year, these mice were analyzed

(J) Flow cytometric analysis of E12.5 fetal liver and blood for cell subsets as indicated gated as in (I). For each analysis, the percentage of total cells that were YFP$^+$ is charted as average ± SEM, n = 10.

(K) Analysis of mice competitively transplanted with 10^6 E12.5 liver cells from TAM-treated (at E9.5) *Mds1*$^{CreERT2/WT}$, *Rosa26*$^{LSL\text{-}YFP/LSL\text{-}YFP}$ mice and 10^5 unlabeled adult bone-marrow cells. Flow cytometric analysis of circulating YFP$^+$ and YFP-negative granulocyte/monocyte cells (CD11b$^+$), B cells (CD19$^+$), and T cells (CD3e$^+$) at 12 weeks post-transplant. See Figure S2F for gating strategy. Average ± SEM, n = 3.

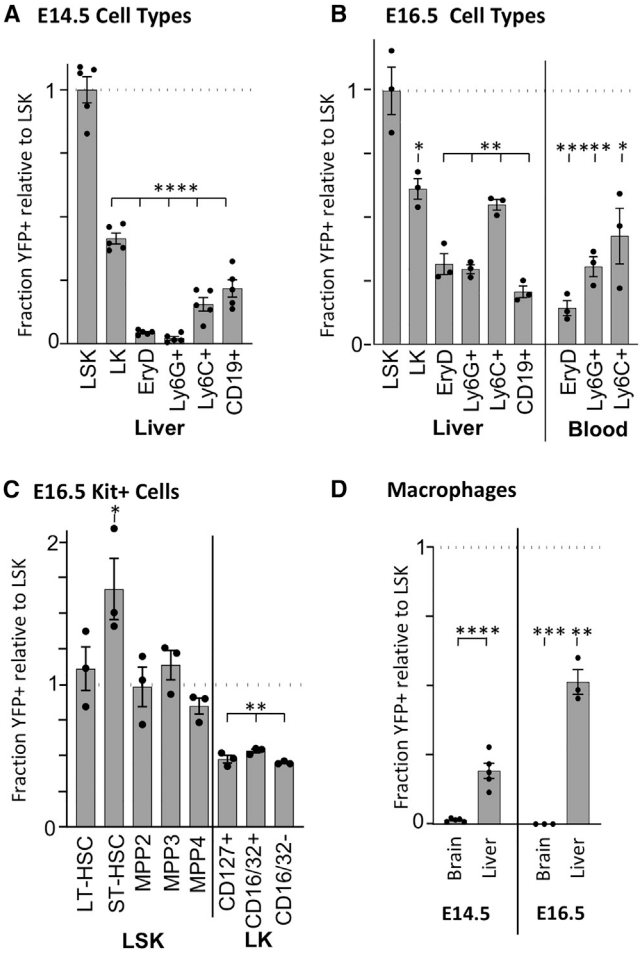

Figure 3. *Mds1*^{CreERT2} *Rosa26*$^{LSL\text{-}YFP}$/E9.5 TAM labeling demonstrates increasing presence of HSC-dependent hematopoiesis through E16.5

(A) Flow cytometric analysis of E14.5 liver cells. Levels of YFP positivity were normalized to the level found in LSK (Lin-Kit$^+$Sca1$^+$, average 23.3% YFP$^+$) to control for excision rates. Averages ± SEM of 5 individual embryos are plotted for LK (Lin-Kit$^+$Sca1$^-$), erythroid (Ter119$^+$FSC^{hi}), granulocyte (Ly6G$^+$), monocyte (Ly6C$^+$), and B (CD19$^+$) cells. See Figures S3A and S3B for gating strategy.

(B) Flow cytometric analysis of circulating blood cells and liver cells at E16.5. Averages ± SEM of 3 individuals are plotted. Gating is as in (A) with the addition of circulating definitive erythroid (EryD, Ter119$^+$) cells gated as in Figure S3C. Levels of YFP positivity were normalized to the level found in LSK average 8.1% YFP$^+$) to control for excision rates.

(C) Flow cytometric analysis of E16.5 progenitors in the liver. LSK was further refined into LT-HSC, ST-HSC, MPP2, MPP3, and MPP4 based on Flt3, CD150, and CD48 positivity (see Figures S3A and S3D). LK were further refined into lymphoid (CD127$^+$), myeloid (CD16/32$^+$), and erythroid/megakaryocyte (CD16/32$^-$) progenitors. Values normalized to YFP levels in LSK (B). Averages ± SEM, n = 3.

(D) Analysis by flow cytometry of YFP$^+$ F4/80$^+$ macrophages from E14.5 and E16.5 brain and liver normalized to YFP positivity of LSK (panels A and B). Details of gating are found in Figure S3E. Average ± SEM, n = 3. Unpaired two tail Student's t test was performed comparing YFP labeling in cell populations to LSK. *p < 0.05; **p < 0.01; ***p < 0.001; ****p < 0.0001.

for YFP$^+$ cells both in blood and in the bone marrow. YFP$^+$ cells constituted nearly a third of the leukocytes in the blood, and similar proportions of bone-marrow immunophenotypic LT-HSCs, MPPs, more restricted hematopoietic progenitors, as well as kit-CD45$^+$ cells (Figures 4A and 4B; Figure S4A). Treatment with TAM at E8.5 did not lead to the labeling of hematopoietic cells in the adult, consistent with lack of pre-HSC labeling at E11.5 (Figure S2E).

We also examined the contribution of HSCs to F4/80$^+$ tissue-resident macrophage populations in the adult. As expected, there was no HSC contribution to microglia, and lower but increasing contribution to macrophages in liver, lung, and kidney (Figure 4C; Figure S4B). Surprisingly, a high proportion of F4/80$^+$ macrophages in the spleen and bone marrow were labeled, indicating that they are predominately HSC-derived. *Mds1*^{CreERT2} *Rosa26*$^{LSL\text{-}YFP}$ activated by TAM at E8.5 did not lead to the labeling of any of these macrophage populations indicating that HSC-independent macrophages are not labeled by the *Mds1*^{creERT2} allele (Figure 4C).

DISCUSSION

HSCs, which transiently emerge in the embryo from hemogenic endothelial cells in large arterial vessels, serve as the foundational source of all circulating blood cells in the postnatal organism. A number of genes, including *Mecom*, *Hlf*, *Procr*, and *HoxA* family members, have been specifically associated with HSC emergence in mice (Iwasaki et al., 2010; Ng et al., 2016; Yokomizo et al., 2019). *Mecom* is one of the most differentially expressed genes present in hemogenic endothelium of the aorta compared both to hemogenic endothelium in the yolk sac and to non-hemogenic endothelial cells (Baron et al., 2018; Gao et al., 2018; Solaimani Kartalaei et al., 2015; Yokomizo et al., 2019). Recently, Mecom expression has been identified in primary murine aortic arterial-identity cells, as well as in their subsequent transition in pseudotime to hemogenic endothelium and preHSC identity cells (Hou et al., 2020; Zhu et al., 2020). The *MECOM* locus is complex, with multiple isoforms expressed from two TSS. Here, we report the development of an *Mds1*^{CreERT2} mouse model that contains a TAM-inducible Cre cassette within the first TSS of the *MECOM* locus. Utilizing an *Mds1*^{lacZ} mouse (Zhang et al., 2011), we found expression of the *LacZ* reporter in a subset of cells of the E9.5 aorta that also express Runx1 (Figures 1G–1I), consistent with the reported expression of *MECOM* in aortic endothelial cells as they transition to hemogenic endothelium (Konantz et al., 2016; Yokomizo et al., 2019; Zhu et al., 2020, Hou, 2020 #42). Our data suggest that the *MECOM* locus is transiently expressed during HSC emergence and subsequently downregulated in the fetal liver, unlike its expression in LSK cells in adult mice (Zhang et al., 2011). Our RNA expression studies in adult tissues revealed that the two TSSs are coordinately regulated (Zhang et al., 2011), and analysis of publicly available transcription factor binding data reveals coordinate binding of transcription factors to the two TSSs, as well as similar histone markings and DNaseI hypersensitive sites (unpublished findings). However, the factors regulating transcription from the *Mds1* and *Evi1* promoters in adults or during development are poorly characterized and are an avenue for future research.

Subsets of myeloid and specialized lymphoid cells are formed in the fetus and self-renew postnatally with little input from adult

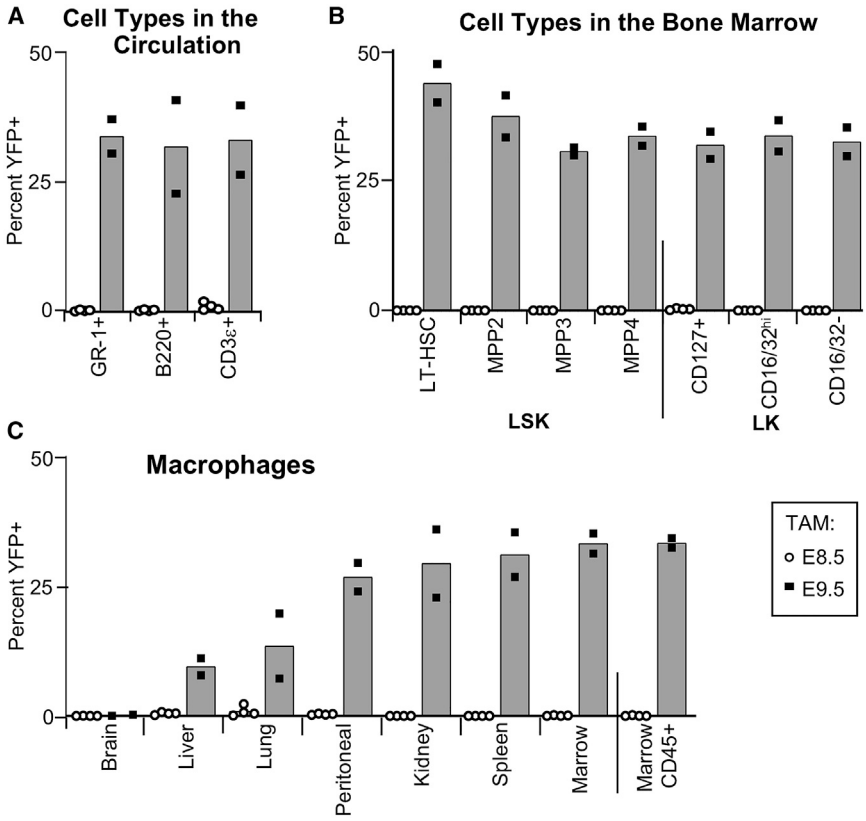

Figure 4. TAM treatment at E9.5 of *Mds1*^{CreERT2} *Rosa26*$^{LSL\text{-}YFP}$ efficiently labels HSCs

(A) Flow cytometric analysis of the proportion of YFP$^+$ granulocyte/monocyte cells (GR-1$^+$), B cells (B220$^+$), and T cells (CD3ε$^+$) in the circulation of 1-year-old *Mds1*^{CreERT2} *Rosa26*$^{LSL\text{-}YFP}$ mice after TAM treatment at E8.5 (empty circles, n = 4) or at E9.5 (solid circles, n = 2).

(B) Flow cytometric analysis of bone marrow of the same mice as in (A) demonstrating a high percentage of YFP$^+$ progenitor cells in LSK subsets, as well as of lineage-restricted lymphoid (CD127$^+$), myeloid (CD16/32$^+$), and erythroid/megakaryocyte (CD16/32$^-$) LK subsets. See Figure S4A for gating strategy. Total marrow CD45$^+$ YFP$^+$ cells shown in (C).

(C) Percentage of YFP$^+$ F4/80$^+$ tissue-resident macrophages in these mice. See Figure S4B for detailed gating strategy. In all panels, the average is plotted.

HSCs (Gentek et al., 2018; Ghosn and Yang, 2015; Hashimoto et al., 2013). The overlapping emergence and lineage output of HSC-independent and HSC-derived hematopoiesis raise important questions regarding the identity and potential functional differences of their mature progeny. Exploring these questions will require ways to distinguish and isolate cells derived from different developmental sources. Current lineage-tracing approaches rely largely on the temporal induction of promoters, including *Cdh5* (*VECadherin*), *Runx1*, *Csf1r*, and *Kit*, that are expressed both in HSC-independent progenitors and also in HSCs (Gomez Perdiguero et al., 2015; Hoeffel et al., 2015; Soares-da-Silva et al., 2021; Stremmel et al., 2018; Zovein et al., 2008). An alternative approach would be to use promoters for genes such as *Hlf*, *Procr,* or *Mecom* that are expressed more specifically in fetal HSCs (Iwasaki et al., 2010; Yokomizo et al., 2019; Yuasa et al., 2005). Although a caveat common to all of these systems, including *Mds1*^{CreERT2}, is that it remains unclear to what degree rare lymphoid or lympho-myeloid progenitors might also be labeled. Our studies reveal the usefulness of the *Mds1*^{CreERT2} *Rosa26*^{LSLYFP} mouse model that labels HSCs as they first emerge from hemogenic endothelium, but does not label the major HSC-independent waves of primitive hematopoietic progenitors and EMPs (Figure S4C).

EMPs begin to colonize the fetal liver between E9.5 and E10.5 and rapidly provide differentiating progeny, particularly the first circulating definitive erythrocytes (McGrath et al., 2015; Palis et al., 1999). Transplantable HSCs subsequently start to seed the liver between E11.5 and E12.5; however, the transition between these two sources of blood cells has only recently begun to be scrutinized (Ema and Nakauchi, 2000; Kumaravelu et al., 2002; Soares-da-Silva et al., 2021). Our analysis of TAM-treated *Mds1*^{CreERT2}*Rosa26*$^{LSL\text{-}YFP}$ embryos indicates that HSCs have begun to generate small numbers of differentiating erythroid, myeloid, and lymphoid progeny between E12.5 and E14.5. By E16.5, a significant proportion of differentiating erythroid, myeloid, and B cell lineage cells in the liver are HSC-derived, and HSCs have now begun to contribute erythroid and myeloid cells to the rapidly expanding pool of circulating blood cells. A similar result was reported in a recent paper that found increased HSC contribution to hematopoiesis from E14.5 to E16.5 (Soares-da-Silva et al., 2021). These authors also observed a strong lineage bias, concluding that erythropoiesis is HSC independent until birth, which we did not observe. This could possibly be due to the challenges of using different lineage-tracing mouse models. Our data support the conclusion that HSCs contribute increasing proportions of erythroid, myeloid, and lymphoid cells to the rapidly developing late gestation murine fetus, supplementing the robust blood cell output of EMPs prior to birth.

Many tissue-resident macrophage populations in adult organs contain contributions of fetal cells that persist by self-renewal. These self-renewing macrophage populations were thought to derive primarily from HSC-independent sources. Here, we used the *Mds1*^{CreERT2}*Rosa26*$^{LSL\text{-}YFP}$ model to examine the contribution of HSCs to F4/80$^+$ macrophage populations in several organs over developmental time. As expected, we found no evidence of HSC contribution to microglia, but increasing contributions of HSCs to macrophages in liver, lung, and kidney (Gomez Perdiguero et al., 2015; Hoeffel et al., 2015; Liu et al., 2019). Interestingly, the majority of F4/80$^+$ cells in the adult spleen and bone marrow, though also

self-maintaining (Hashimoto et al., 2013), appear to be predominantly derived from fetal HSCs (Figure 4C). Macrophage cells in the marrow perform multiple functions, including regulation of the HSC niche, support of erythroid precursor maturation in erythroblastic islands, and clearance of pyrenocytes. The surprisingly high proportion of HSC-derived F4/80^{+} cells in the fetal compared to the adult liver may reflect the need for those macrophage cells to also fulfill these specific functions in the fetus.

STAR★METHODS

Detailed methods are provided in the online version of this paper and include the following:

- KEY RESOURCES TABLE
- RESOURCE AVAILABILITY
  - Lead contact
  - Material availability
  - Data and code availability
- EXPERIMENTAL MODEL AND SUBJECT DETAILS
  - Mice
- METHOD DETAILS
  - Construction of Mds1^{CreERT2} allele
  - Time pregnancy and competitive BM transplantation
  - Tissue collection and processing
  - Histochemical and β-galactosidase staining
  - Runx1 Immunohistochemistry
  - Flow cytometric analysis
- QUANTITATION AND STATISTICAL ANALYSIS

SUPPLEMENTAL INFORMATION

Supplemental information can be found online at https://doi.org/10.1016/j.celrep.2021.109562.

ACKNOWLEDGMENTS

Funding: NIH NCI R01CA175761 and R01CA120313 (to A.S.P.), NIH R01 DK119285 (to J.P.), NYSTEM Grant C029547 (to Y.Z.), and the Department of Pathology and Laboratory Medicine, University of Rochester Medical Center (to A.S.P. and Y.Z.). We thank Stacey Duemmel, Leah Vit, Emma R. Guilfoyle, and Anne Koniski for technical assistance and the URMC Flow Cytometry Core Facility for technical support.

AUTHOR CONTRIBUTIONS

Y.Z., K.E.M., E.A., P.D.K., H.Y., K.F., K.A.M., S.R., and A.S.P. performed experiments and analyzed data. Y.Z., K.E.M., J.P., and A.S.P. wrote the manuscript.

DECLARATION OF INTERESTS

The authors declare no competing interests.

Received: May 7, 2020
Revised: May 24, 2021
Accepted: July 28, 2021
Published: August 17, 2021

REFERENCES

Amend, S.R., Valkenburg, K.C., and Pienta, K.J. (2016). Murine Hind Limb Long Bone Dissection and Bone Marrow Isolation. J. Vis. Exp. Published online April 14, 2021. https://doi.org/10.3791/53936.

Asari, S., Okada, S., Ohkubo, Y., Sakamoto, A., Arima, M., Hatano, M., Kuroda, Y., and Tokuhisa, T. (2004). Beta-galactosidase of ROSA26 mice is a useful marker for detecting the definitive erythropoiesis after stem cell transplantation. Transplantation *78*, 516–523.

Azzoni, E., Frontera, V., McGrath, K.E., Harman, J., Carrelha, J., Nerlov, C., Palis, J., Jacobsen, S.E.W., and de Bruijn, M.F. (2018). Kit ligand has a critical role in mouse yolk sac and aorta-gonad-mesonephros hematopoiesis. EMBO Rep. *19*, e45477.

Balounová, J., Šplíchalová, I., Dobešová, M., Kolář, M., Fišer, K., Procházka, J., Sedlacek, R., Jurisicova, A., Sung, H.K., Kořínek, V., et al. (2019). Toll-like receptor 2 expression on c-kit^{+} cells tracks the emergence of embryonic definitive hematopoietic progenitors. Nat. Commun. *10*, 5176.

Baron, C.S., Kester, L., Klaus, A., Boisset, J.-C., Thambyrajah, R., Yvernogeau, L., Kouskoff, V., Lacaud, G., van Oudenaarden, A., and Robin, C. (2018). Single-cell transcriptomics reveal the dynamic of haematopoietic stem cell production in the aorta. Nat. Commun. *9*, 2517.

Beaudin, A.E., Boyer, S.W., Perez-Cunningham, J., Hernandez, G.E., Derderian, S.C., Jujjavarapu, C., Aaserude, E., MacKenzie, T., and Forsberg, E.C. (2016). A Transient Developmental Hematopoietic Stem Cell Gives Rise to Innate-like B and T Cells. Cell Stem Cell *19*, 768–783.

Bitter, M.A., Neilly, M.E., Le Beau, M.M., Pearson, M.G., and Rowley, J.D. (1985). Rearrangements of chromosome 3 involving bands 3q21 and 3q26 are associated with normal or elevated platelet counts in acute nonlymphocytic leukemia. Blood *66*, 1362–1370.

Böiers, C., Carrelha, J., Lutteropp, M., Luc, S., Green, J.C., Azzoni, E., Woll, P.S., Mead, A.J., Hultquist, A., Swiers, G., et al. (2013). Lymphomyeloid contribution of an immune-restricted progenitor emerging prior to definitive hematopoietic stem cells. Cell Stem Cell *13*, 535–548.

Christodoulou, C., Spencer, J.A., Yeh, S.A., Turcotte, R., Kokkaliaris, K.D., Panero, R., Ramos, A., Guo, G., Seyedhassantehrani, N., Esipova, T.V., et al. (2020). Live-animal imaging of native haematopoietic stem and progenitor cells. Nature *578*, 278–283.

Ema, H., and Nakauchi, H. (2000). Expansion of hematopoietic stem cells in the developing liver of a mouse embryo. Blood *95*, 2284–2288.

Fears, S., Mathieu, C., Zeleznik-Le, N., Huang, S., Rowley, J.D., and Nucifora, G. (1996). Intergenic splicing of MDS1 and EVI1 occurs in normal tissues as well as in myeloid leukemia and produces a new member of the PR domain family. Proc. Natl. Acad. Sci. USA *93*, 1642–1647.

Frame, J.M., Fegan, K.H., Conway, S.J., McGrath, K.E., and Palis, J. (2016). Definitive Hematopoiesis in the Yolk Sac Emerges from Wnt-Responsive Hemogenic Endothelium Independently of Circulation and Arterial Identity. Stem Cells *34*, 431–444.

Gao, L., Tober, J., Gao, P., Chen, C., Tan, K., and Speck, N.A. (2018). RUNX1 and the endothelial origin of blood. Exp. Hematol. *68*, 2–9.

Gao, P., Chen, C., Howell, E.D., Li, Y., Tober, J., Uzun, Y., He, B., Gao, L., Zhu, Q., Siekmann, A.F., et al. (2020). Transcriptional regulatory network controlling the ontogeny of hematopoietic stem cells. Genes Dev. *34*, 950–964.

Gentek, R., Ghigo, C., Hoeffel, G., Bulle, M.J., Msallam, R., Gautier, G., Launay, P., Chen, J., Ginhoux, F., and Bajénoff, M. (2018). Hemogenic Endothelial Fate Mapping Reveals Dual Developmental Origin of Mast Cells. Immunity *48*, 1160–1171.

Ghosn, E.E., and Yang, Y. (2015). Hematopoietic stem cell-independent B-1a lineage. Ann. N Y Acad. Sci. *1362*, 23–38.

Gomez Perdiguero, E., Klapproth, K., Schulz, C., Busch, K., Azzoni, E., Crozet, L., Garner, H., Trouillet, C., de Bruijn, M.F., Geissmann, F., and Rodewald, H.R. (2015). Tissue-resident macrophages originate from yolk-sac-derived erythro-myeloid progenitors. Nature *518*, 547–551.

Goyama, S., Yamamoto, G., Shimabe, M., Sato, T., Ichikawa, M., Ogawa, S., Chiba, S., and Kurokawa, M. (2008). Evi-1 is a critical regulator for hematopoietic stem cells and transformed leukemic cells. Cell Stem Cell *3*, 207–220.

Hashimoto, D., Chow, A., Noizat, C., Teo, P., Beasley, M.B., Leboeuf, M., Becker, C.D., See, P., Price, J., Lucas, D., et al. (2013). Tissue-resident macrophages self-maintain locally throughout adult life with minimal contribution from circulating monocytes. Immunity *38*, 792–804.

Hoeffel, G., Chen, J., Lavin, Y., Low, D., Almeida, F.F., See, P., Beaudin, A.E., Lum, J., Low, I., Forsberg, E.C., et al. (2015). C-Myb(+) erythro-myeloid progenitor-derived fetal monocytes give rise to adult tissue-resident macrophages. Immunity *42*, 665–678.

Hohenauer, T., and Moore, A.W. (2012). The Prdm family: expanding roles in stem cells and development. Development *139*, 2267–2282.

Hou, S., Li, Z., Zheng, X., Gao, Y., Dong, J., Ni, Y., Wang, X., Li, Y., Ding, X., Chang, Z., et al. (2020). Embryonic endothelial evolution towards first hematopoietic stem cells revealed by single-cell transcriptomic and functional analyses. Cell Res. *30*, 376–392.

Hoyt, P.R., Bartholomew, C., Davis, A.J., Yutzey, K., Gamer, L.W., Potter, S.S., Ihle, J.N., and Mucenski, M.L. (1997). The *Evi1* proto-oncogene is required at midgestation for neural, heart, and paraxial mesenchyme development. Mech. Dev. *65*, 55–70.

Iwasaki, H., Arai, F., Kubota, Y., Dahl, M., and Suda, T. (2010). Endothelial protein C receptor-expressing hematopoietic stem cells reside in the perisinusoidal niche in fetal liver. Blood *116*, 544–553.

Juneja, S.C., Vonica, A., Zeiss, C., Lezon-Geyda, K., Yatsula, B., Sell, D.R., Monnier, V.M., Lin, S., Ardito, T., Eyre, D., et al. (2014). Deletion of Mecom in mouse results in early-onset spinal deformity and osteopenia. Bone *60*, 148–161.

Kingsley, P.D., Malik, J., Fantauzzo, K.A., and Palis, J. (2004). Yolk sac-derived primitive erythroblasts enucleate during mammalian embryogenesis. Blood *104*, 19–25.

Konantz, M., Alghisi, E., Müller, J.S., Lenard, A., Esain, V., Carroll, K.J., Kanz, L., North, T.E., and Lengerke, C. (2016). Evi1 regulates Notch activation to induce zebrafish hematopoietic stem cell emergence. EMBO J. *35*, 2315–2331.

Kumaravelu, P., Hook, L., Morrison, A.M., Ure, J., Zhao, S., Zuyev, S., Ansell, J., and Medvinsky, A. (2002). Quantitative developmental anatomy of definitive haematopoietic stem cells/long-term repopulating units (HSC/RUs): role of the aorta-gonad-mesonephros (AGM) region and the yolk sac in colonisation of the mouse embryonic liver. Development *129*, 4891–4899.

Liu, P., Jenkins, N.A., and Copeland, N.G. (2003). A highly efficient recombineering-based method for generating conditional knockout mutations. Genome Res. *13*, 476–484.

Liu, Z., Gu, Y., Chakarov, S., Bleriot, C., Kwok, I., Chen, X., Shin, A., Huang, W., Dress, R.J., Dutertre, C.A., et al. (2019). Fate Mapping via Ms4a3-Expression History Traces Monocyte-Derived Cells. Cell *178*, 1509–1525.

Loughna, S., and Henderson, D. (2007). Methodologies for staining and visualisation of beta-galactosidase in mouse embryos and tissues. Methods Mol. Biol. *411*, 1–11.

Luis, T.C., Luc, S., Mizukami, T., Boukarabila, H., Thongjuea, S., Woll, P.S., Azzoni, E., Giustacchini, A., Lutteropp, M., Bouriez-Jones, T., et al. (2016). Initial seeding of the embryonic thymus by immune-restricted lympho-myeloid progenitors. Nat. Immunol. *17*, 1424–1435.

Lux, C.T., Yoshimoto, M., McGrath, K., Conway, S.J., Palis, J., and Yoder, M.C. (2008). All primitive and definitive hematopoietic progenitor cells emerging before E10 in the mouse embryo are products of the yolk sac. Blood *111*, 3435–3438.

Ma, X., Robin, C., Ottersbach, K., and Dzierzak, E. (2002). The Ly-6A (Sca-1) GFP transgene is expressed in all adult mouse hematopoietic stem cells. Stem Cells *20*, 514–521.

McGrath, K.E., Frame, J.M., Fromm, G.J., Koniski, A.D., Kingsley, P.D., Little, J., Bulger, M., and Palis, J. (2011). A transient definitive erythroid lineage with unique regulation of the β-globin locus in the mammalian embryo. Blood *117*, 4600–4608.

McGrath, K.E., Frame, J.M., Fegan, K.H., Bowen, J.R., Conway, S.J., Catherman, S.C., Kingsley, P.D., Koniski, A.D., and Palis, J. (2015). Distinct Sources of Hematopoietic Progenitors Emerge before HSCs and Provide Functional Blood Cells in the Mammalian Embryo. Cell Rep. *11*, 1892–1904.

Metzger, D., Clifford, J., Chiba, H., and Chambon, P. (1995). Conditional site-specific recombination in mammalian cells using a ligand-dependent chimeric Cre recombinase. Proc. Natl. Acad. Sci. USA *92*, 6991–6995.

Morishita, K., Parker, D.S., Mucenski, M.L., Jenkins, N.A., Copeland, N.G., and Ihle, J.N. (1988). Retroviral activation of a novel gene encoding a zinc finger protein in IL-3-dependent myeloid leukemia cell lines. Cell *54*, 831–840.

Mu, J., Slevin, J.C., McCormick, S., and Adamson, S.L. (2008). In vivo quantification of embryonic and placental growth during gestation in mice using micro-ultrasound. Reprod. Biol. Endocrinol. *6*, 34.

Mucenski, M.L., Taylor, B.A., Ihle, J.N., Hartley, J.W., Morse, H.C., 3rd, Jenkins, N.A., and Copeland, N.G. (1988). Identification of a common ecotropic viral integration site, Evi-1, in the DNA of AKXD murine myeloid tumors. Mol. Cell. Biol. *8*, 301–308.

Nagy, A., Gertsenstein, M., Vintersten, K., and Behringer, R. (2007). Staining Whole Mouse Embryos for beta-Galactosidase (lacZ) Activity. CSH Protoc. *2007*, pdb.prot4725.

Ng, E.S., Azzola, L., Bruveris, F.F., Calvanese, V., Phipson, B., Vlahos, K., Hirst, C., Jokubaitis, V.J., Yu, Q.C., Maksimovic, J., et al. (2016). Differentiation of human embryonic stem cells to HOXA^{+} hemogenic vasculature that resembles the aorta-gonad-mesonephros. Nat. Biotechnol. *34*, 1168–1179.

Palis, J., and Yoder, M.C. (2001). Yolk-sac hematopoiesis: the first blood cells of mouse and man. Exp. Hematol. *29*, 927–936.

Palis, J., Robertson, S., Kennedy, M., Wall, C., and Keller, G. (1999). Development of erythroid and myeloid progenitors in the yolk sac and embryo proper of the mouse. Development *126*, 5073–5084.

Perkins, A.S., Mercer, J.A., Jenkins, N.A., and Copeland, N.G. (1991). Patterns of Evi-1 expression in embryonic and adult tissues suggest that Evi-1 plays an important regulatory role in mouse development. Development *111*, 479–487.

Pronk, C.J., Rossi, D.J., Månsson, R., Attema, J.L., Norddahl, G.L., Chan, C.K., Sigvardsson, M., Weissman, I.L., and Bryder, D. (2007). Elucidation of the phenotypic, functional, and molecular topography of a myeloerythroid progenitor cell hierarchy. Cell Stem Cell *1*, 428–442.

Qian, B.Z., Li, J., Zhang, H., Kitamura, T., Zhang, J., Campion, L.R., Kaiser, E.A., Snyder, L.A., and Pollard, J.W. (2011). CCL2 recruits inflammatory monocytes to facilitate breast-tumour metastasis. Nature *475*, 222–225.

Rubin, C.M., Larson, R.A., Anastasi, J., Winter, J.N., Thangavelu, M., Vardiman, J.W., Rowley, J.D., and Le Beau, M.M. (1990). t(3;21)(q26;q22): a recurring chromosomal abnormality in therapy-related myelodysplastic syndrome and acute myeloid leukemia. Blood *76*, 2594–2598.

Samokhvalov, I.M., Samokhvalova, N.I., and Nishikawa, S. (2007). Cell tracing shows the contribution of the yolk sac to adult haematopoiesis. Nature *446*, 1056–1061.

Sanes, J.R., Rubenstein, J.L., and Nicolas, J.F. (1986). Use of a recombinant retrovirus to study post-implantation cell lineage in mouse embryos. EMBO J. *5*, 3133–3142.

Soares-da-Silva, F., Freyer, L., Elsaid, R., Burlen-Defranoux, O., Iturri, L., Sismeiro, O., Pinto-do-Ó, P., Gomez-Perdiguero, E., and Cumano, A. (2021). Yolk sac, but not hematopoietic stem cell-derived progenitors, sustain erythropoiesis throughout murine embryonic life. J. Exp. Med. *218*, e20201729.

Solaimani Kartalaei, P., Yamada-Inagawa, T., Vink, C.S., de Pater, E., van der Linden, R., Marks-Bluth, J., van der Sloot, A., van den Hout, M., Yokomizo, T., van Schaick-Solernó, M.L., et al. (2015). Whole-transcriptome analysis of endothelial to hematopoietic stem cell transition reveals a requirement for Gpr56 in HSC generation. J. Exp. Med. *212*, 93–106.

Srinivas, S., Watanabe, T., Lin, C.S., William, C.M., Tanabe, Y., Jessell, T.M., and Costantini, F. (2001). Cre reporter strains produced by targeted insertion of EYFP and ECFP into the ROSA26 locus. BMC Dev. Biol. *1*, 4.

Stremmel, C., Schuchert, R., Wagner, F., Thaler, R., Weinberger, T., Pick, R., Mass, E., Ishikawa-Ankerhold, H.C., Margraf, A., Hutter, S., et al. (2018). Yolk sac macrophage progenitors traffic to the embryo during defined stages of development. Nat. Commun. *9*, 75.

Yokomizo, T., and Dzierzak, E. (2010). Three-dimensional cartography of hematopoietic clusters in the vasculature of whole mouse embryos. Development *137*, 3651–3661.

Yokomizo, T., Watanabe, N., Umemoto, T., Matsuo, J., Harai, R., Kihara, Y., Nakamura, E., Tada, N., Sato, T., Takaku, T., et al. (2019). Hlf marks the developmental pathway for hematopoietic stem cells but not for erythro-myeloid progenitors. J. Exp. Med. *216*, 1599–1614.

Yoshimoto, M., Montecino-Rodriguez, E., Ferkowicz, M.J., Porayette, P., Shelley, W.C., Conway, S.J., Dorshkind, K., and Yoder, M.C. (2011). Embryonic day 9 yolk sac and intra-embryonic hemogenic endothelium independently generate a B-1 and marginal zone progenitor lacking B-2 potential. Proc. Natl. Acad. Sci. USA *108*, 1468–1473.

Yoshimoto, M., Porayette, P., Glosson, N.L., Conway, S.J., Carlesso, N., Cardoso, A.A., Kaplan, M.H., and Yoder, M.C. (2012). Autonomous murine T-cell progenitor production in the extra-embryonic yolk sac before HSC emergence. Blood *119*, 5706–5714.

Yuasa, H., Oike, Y., Iwama, A., Nishikata, I., Sugiyama, D., Perkins, A., Mucenski, M.L., Suda, T., and Morishita, K. (2005). Oncogenic transcription factor Evi1 regulates hematopoietic stem cell proliferation through GATA-2 expression. EMBO J. *24*, 1976–1987.

Yzaguirre, A.D., de Bruijn, M.F., and Speck, N.A. (2017). The Role of Runx1 in Embryonic Blood Cell Formation. Adv. Exp. Med. Biol. *962*, 47–64.

Zambrowicz, B.P., Imamoto, A., Fiering, S., Herzenberg, L.A., Kerr, W.G., and Soriano, P. (1997). Disruption of overlapping transcripts in the ROSA beta geo 26 gene trap strain leads to widespread expression of beta-galactosidase in mouse embryos and hematopoietic cells. Proc. Natl. Acad. Sci. USA *94*, 3789–3794.

Zhang, Y., Stehling-Sun, S., Lezon-Geyda, K., Juneja, S.C., Coillard, L., Chatterjee, G., Wuertzer, C.A., Camargo, F., and Perkins, A.S. (2011). PR-domain-containing Mds1-Evi1 is critical for long-term hematopoietic stem cell function. Blood *118*, 3853–3861.

Zhao, T., Zhou, X., Szabó, N., Leitges, M., and Alvarez-Bolado, G. (2007). Foxb1-driven Cre expression in somites and the neuroepithelium of diencephalon, brainstem, and spinal cord. Genesis *45*, 781–787.

Zhu, Q., Gao, P., Tober, J., Bennett, L., Chen, C., Uzun, Y., Li, Y., Howell, E.D., Mumau, M., Yu, W., et al. (2020). Developmental trajectory of prehematopoietic stem cell formation from endothelium. Blood *136*, 845–856.

Zovein, A.C., Hofmann, J.J., Lynch, M., French, W.J., Turlo, K.A., Yang, Y., Becker, M.S., Zanetta, L., Dejana, E., Gasson, J.C., et al. (2008). Fate tracing reveals the endothelial origin of hematopoietic stem cells. Cell Stem Cell *3*, 625–636.

STAR★METHODS

KEY RESOURCES TABLE

Reagent or resource	Source	Identifier
Antibodies		
Hamster Anti-Mouse CD3e PE-CF594 Clone 145-2C11	BD	(BD Biosciences Cat# 562286, RRID:AB_11153307)
Anti-Mouse CD3e PE Clone 145-2C11	eBioscience	Cat# 17-0031-82
Anti-Mouse CD3e APC-AF780 Clone 17A2	eBioscience	Cat# 47-0032-82
Rat Anti Mouse -CD11b APC Clone M1/70	BD	(BD Biosciences Cat# 553312, RRID:AB_398535)
Rat Anti Mouse -CD11b APC-EF780 Clone M1/70	eBioscience	Cat# 27-0112-82
Rat Anti Mouse CD11b PEcy7 Clone M1/70	BD	(BD Biosciences Cat# 561098, RRID:AB_2033994)
Anti-Mouse CD16/32 PE Clone 93	eBioscience	Cat# 12-0161-82
Anti-Mouse CD16/32 PEcy7 Clone 93	eBioscience	Cat# 25-0161-81
Rat Anti-Mouse CD16/CD32 APC-Cy7 Clone 2.4G2	BD	(BD Biosciences Cat# 560541, RRID:AB_1645229)
Rat Anti-mouse CD19 APCeFluor780 Clone ID3	eBioscience	Cat# 47-0193-82
Rat Anti-mouse CD19 PE Clone ID3	eBioscience	Cat# 12-0193-82
Rat Anti-mouse CD19 PerCP-Cy5.5 Clone ID3	eBioscience	Cat #25-0193-82
Rat Anti-Mouse CD34 AF700 Clone RAM34	BD	(BD Biosciences Cat# 560518, RRID:AB_1727471)
Rat Anti-Mouse CD45 PE Clone 30-F11	eBioscience	Cat #12-0451-82
Rat Anti-Mouse CD45R/B220 PE-Cy7 Clone RA3-6B2	BD	(BD Biosciences Cat# 552772, RRID:AB_394458)
Armenian Hamster anti-Mouse CD48 PE, Clone: HM48-1,	eBioscience	Cat# 12-0481-81
Armenian Hamster anti-Mouse CD48 APC-eFluor780, Clone: HM48-1,	eBioscience	Cat# 50-112-4034
Rat Anti-Mouse CD115 (CSF1R) PE clone AFS98	eBioscience	Cat# 12-1152-82
Rat Anti-Mouse CD117 (Kit) PE-cy5, Clone: 2B8	eBioscience	Cat# 50-140-92
Rat Anti-Mouse CD117 (Kit) PE Clone: 2B8	eBioscience	Cat #12-1171-82
Rat Anti-Mouse CD117 (Kit) PECF594 Clone: 2B8	BD	(BD Biosciences Cat# 562417, RRID:AB_11154233)
Rat Anti-Mouse CD117 (Kit) PE-cy7, Clone: 2B8	eBioscience	Cat #25-1171-82
Rat Anti-Mouse CD127 BUV737 Clone SB/199	BD	(BD Biosciences Cat# 612841, RRID:AB_2870163)
Rat Anti-Mouse CD127 APC clone A7R34	eBioscience	Cat#17-1271-82
Rat anti-Mouse CD135 (Flt3) PE, Clone: A2F10	eBioscience	Cat# 50-106-20
Rat anti-Mouse CD135 (Flt3) PE-CF594, Clone: A2F10	BD	(BD Biosciences Cat# 562537, RRID:AB_2737639)
Rat anti-Mouse CD144 (VECadherin) EF660 Clone BV13	eBioscience	Cat#50-106-20
Rat anti-Mouse CD150 APC Clone: 9D1	eBioscience	Cat# 50-150-87
Rat Anti-mouse F4/80 APC Clone BM8	eBioscience	Cat #17-4801-82
Rat Anti-Mouse GR1 (Ly-6G and Ly6C) APC-Cy7 Clone RB6-8C5	BD	(BD Biosciences Cat# 557661, RRID:AB_396775)
Rat Anti-mouse Ly6C APC Clone HK1.4	eBioscience	Cat #17-5932-82
Rat Anti-mouse Ly6C PEcy7 Clone HK1.4	eBioscience	Cat #25-5932-82
Rat antimouse Sca-1 (Ly-6A/E) PerCP-Cy5.5, Clone: D7	eBioscience	Cat# 50-158-66

(*Continued on next page*)

Continued		
Reagent or resource	Source	Identifier
Rat Anti-Mouse Ter119 Percp cy5.5 Clone TER-119	BD	(BD Biosciences Cat# 560512, RRID:AB_10561844)
Rat Anti-Mouse Ter119 APC-eFluor780 Clone TER-119	eBioscience	Cat # 47-5921-80
Rabbit anti-Runx	Abcam	(Abcam Cat# ab92336, RRID:AB_2049267)
Goat anti-rabbit IgG AF647	ThermoFisher	(Thermo Fisher Scientific Cat# A-21244, RRID:AB_2535812)
ProLong Gold antifade reagent	ThermoFisher	Cat # P36934
Bacterial and Virus Strains		
bacterial line DY380	Neal Copeland (Liu et al., 2003)	n/a
Chemicals, Peptides, and Recombinant Proteins		
PE-CF594 Streptavidin	BD Biosciences	Cat# 562318
Tamoxifen (CAS 10540-29-1)	Santa Cruz Biotechnology	Cat# sc-208414
DAPI	Thermofisher	Cat# EN62248
Critical Commercial Assays		
SuperScript IV One-Step RT-PCR System	Thermofisher	Cat# 12594025
GoTaq	Promega	Cat# M7422
Experimental Models: Organisms/Strains		
B6.129X1-*Gt(ROSA)26Sor*$^{tm1(EYFP)Cos}$*/J*	Jackson Lab	Stock No: 006148
B6.129S4-*Gt(ROSA)*$^{26Sortm1(FLP1)Dym}$*/RainJ*	Jackson Lab	Stock No: 009086
Mds1^{CreEr}	This paper	n/a
Mds1^{LacZ}	This paper	n/a
C57BL/6 wildtype Inbred mice	Charles River	C57BL/6NCrl
Oligonucleotides		
M2 wtfw GGTGTCCAAACTGACAATGC	This paper	n/a
M2 fw ACTCACCCTGAAGTTCTCAGG	This paper	n/a
M2 rv CGGAGTTGCCACAGCTGG	This paper	n/a
YFP fw AAAGTCGCTCTGAGTTGTTAT	This paper	n/a
YFP rv AAGACCGCGAAGAGTTTGTC	This paper	n/a
Recombinant DNA		
BAC RP24-120B18	BACPAC Resources Center (BPRC)	RP24-120B18
GS1650	This paper	n/a
GS1656	This paper	n/a
GS1690	This paper	n/a
Software and Algorithms		
FlowJo 8.5.3 software (TreeStar)	BD	FJ8.5.3

RESOURCE AVAILABILITY

Lead contact

Further information and requests for resources should be directed to Archibald Perkins (archibald_perkins@urmc.rochester.edu).

Material availability

Mds1^{lacZ} mice (also referred to as *Mds1*^{m1} mice) have been submitted to MMRRC (Mds1-lacZ, Stock No. MMRRC:68126); please contact the MMRRC regarding availability. *Mds1*^{CreERT2} mice (also referred to as *Mds1*^{m2} mice) have been submitted to Jackson Labs for distribution (Mds1-CreERT2, Stock No. 032863). Please contact Jen Merriman regarding availability (Jen.Merriam@jax.org). There are no restrictions on the distribution of these lines.

Data and code availability

- Any data reported in this paper will be shared by the lead contact upon request.
- This paper does not report any original code.
- Any additional information requires to reanalyze the data reported in this paper is available from the lead contact upon request.

EXPERIMENTAL MODEL AND SUBJECT DETAILS

Mice

Mds1^{lacZ} mice have been described previously (Zhang et al., 2011). *Mds1*^{CreERT2} (also referred to as *Mds1*^{m2}) mice were generated as described below. Rosa26-YFP reporter mice (Srinivas et al., 2001) *Gt(ROSA)26Sor*$^{tm1(EYFP)Cos/J}$, Stock No: 006148, abbreviated *Rosa26*^{YFP}) and C57BL/6 were obtained from Jackson Labs. Both female and male embryos and adults were analyzed in these experiments. For timed pregnancies, dams were aged 6-16 weeks; sires were aged 7-60 weeks. For bone marrow transplantation, recipient mice were aged 8-12 weeks. All animals were housed and cared for in facilities operated by the Division of Animal Care at the University of Rochester Medical Center and used in accordance with the guidelines of the University of Rochester School of Medicine and Dentistry Institutional Animal Care and Use Committee.

METHOD DETAILS

Construction of Mds1^{CreERT2} allele

Plasmid construction was carried out using BAC recombineering (Liu et al., 2003). Bacterial artificial chromosome for *Mecom* (clone RP24-120B18) was introduced via electroporation into bacterial strain DY380 to create GS1650. The ApSacB cassette was then inserted into exon 1 of *Mecom* destroying the exon's splice donor to create GS1656. The CreERT2 cassette (Metzger et al., 1995), derived from plasmid pXL119 (Zhao et al., 2007), together with a FRT-neo-FRT cassette, was inserted into GS1656, replacing the ApSacB cassette, to create GS1690. The PciI site of plasmid pL253 (Liu et al., 2003) was changed to an NsiI site, creating p1342. The NotI site of p1342 was altered to a FseI site, creating p1343. The NsiI fragment of GS1690 was then transferred into p1343 to create the final plasmid, p1347, which was linearized with FseI and submitted to the Genome Editing Facility at the University of Rochester, which created embryonic stem cell clones that were screened by Southern blotting, cutting DNAs with EcoRV for both the 5′ and 3′ hybridization probes. Ten positives were identified from 192 clones, one of which was used to create mice. These were then crossed with a FLPE deleter strain (*Gt(ROSA)26Sor*$^{tm1(FLP1)Dym/RainJ)}$ to delete the Frt-neo-Frt cassette; the resultant allele was designated *Mds1*^{CreERT2}.

Time pregnancy and competitive BM transplantation

Time pregnancy experiments were setup using male *Mds1*$^{+/CreERT2}$ *Rosa26*$^{LSL\text{-}YFP/LSL\text{-}YFP}$ crossed with *Rosa26*$^{LSL\text{-}YFP}$ or C57BL/6 females. Mice were mated overnight and the morning of vaginal plug detection was considered embryonic day (E) 0.3. Pregnant mice were treated with tamoxifen (TAM) freshly dissolved in corn oil at 10mg/ml and 1mg/mouse delivered by gavage at E7.5, E8.5 or E9.5, and harvested at E11.5, E12.5, E14.5 or E16.5 for tracing embryonic hematopoiesis, or harvested 12 months after birth for long term tracing experiments. For competitive repopulation assays, C57BL/6 recipient mice were given 10 Gy of radiation, split in two 5-Gy doses separated by 24 hours and injected i.v. with 2×10^6 E12.5 liver cells mixed with 100,000 C57BL/6 control bone marrow cells

Tissue collection and processing

For complete blood count (CBC) values, blood was collected by capillary action by holding a heparinized 147 mm glass blood collection tube to a razor-pricked mouse tail. CBC measurements on fresh blood samples were taken using a scil Vet ABC Plus+ hematology analyzer.

Marrow cells were collected from mouse tibias and femurs as follows. Mice were euthanized with carbon dioxide and cervical dislocation, and tibias and femurs were dissected free of muscle, tendons, and connective tissue (Amend et al., 2016) and placed into room temperature sterile phosphate-buffered saline (PBS). Marrow contents were flushed from femurs with 1 mL of PBS by cutting the bones at the distal ends of the central marrow cavity. Pooled marrow contents in PBS were washed once with PBS and used in subsequent hematopoietic analyses (see section below: Flow Cytometry).

Embryonic tissues were isolated from staged embryos were dissected from dams as follows. Dams were euthanized with carbon dioxide and cervical dislocation. Uteri were removed from the peritoneum and washed with several changes of phosphate-buffered saline (PBS). Embryos were dissected free of decidual tissues and Reichert's membrane in IMDM/PBS with 0.2% delipidated BSA using #5 watchmakers forceps (Dumoxal; Electron Microscopy Science, Ft. Washington, PA). Vestiges of maternal blood cells were removed by multiple transfers of tissues into fresh medium during the dissection process. Somite stage embryos (E8.25-E11.5) were grouped according to somite number. Most of the blood was derived from the larger vessels of the embryo proper. At E > 11.5, the liver was isolated separately from the remainder of the embryo proper. Embryonic livers were dissociated with Type I Collagenase

(Stem Cell Technologies, diluted 1:3 with Dulbecco's Phosphate Buffered Saline (DPBS or PB2), with 0.1 g/L CaCl2, 0.3% BSA (Gemini Bio-Products) and 0.1% glucose with gentle pipetting (McGrath et al., 2011). Cells were counted and used for Flow Cytometry (see below) or transplantation into irradiated recipient mice (see Competitive BM transplantation section above).

Histochemical and β-galactosidase staining

Timed pregnancies between dams and sires of appropriate genotypes. Embryos at different stages were harvested and dissected clear of yolk sac, amniotic tissue, and placenta. β-galactosidase staining (Loughna and Henderson, 2007; Nagy et al., 2007; Sanes et al., 1986) of whole-mount embryos was performed as follows: Embryos were fixed in 0.4% paraformaldehyde (in PBS, pH 7.4) on ice for 15 minutes for embryos up to E12.5 dpc and for 30 min for E13.5-E14.5. Following fixation, embryos were rinsed 3 times in PBS. Embryos were then stained in 2 mM $MgCl_2$, 0.02% IGEPAL, 0.1 M phosphate buffer pH 7.2, 5 mM potassium ferricyanide, 5 mM potassium ferrocyanide, 0.01% sodium deoxycholate, and 1 mg/ml X-gal in a 24-well tissue culture plate, incubating at 37°C in a humidified tissue culture incubator until color develops (2-8 hr). After the staining is complete, embryos were rinsed 4-5 times in PBS, then post-fixed in 2% paraformaldehyde/PBS overnight at 4°C. Embryos were then stored in 70% ethanol. Whole-mount photography was performed on a Zeiss 9901 Stereo Zoom microscope. Embryos were then dehydrated, embedded in paraffin, sectioned, and counterstained with eosin. Slides were then dehydrated and coverslipped.

Runx1 Immunohistochemistry

β-galactosidase-stained sections were hydrated, treated with 3% hydrogen peroxide, and subjected to HIER with 10mM Citric acid pH6, 0.05% Tween. Sections were blocked in PBST with 5% BSA and 5% goat serum, incubated overnight at 4°C with Rabbit anti-Runx1 (Abcam Ab92336), washed and incubated with an AF647 secondary antibody (Thermofisher A-21244). Sections were counterstained with DAPI and mounted in antifade Prolong Gold.

Flow cytometric analysis

All antibody used in this study are listed in Key Resources Table and combinations and gating are shown in Supplemental Figures. Flow cytometry was performed on a LSRii or LSR Fortessa X20 (BD Biosciences) and analyzed with FlowJo v10.3 software (TreeStar).

QUANTITATION AND STATISTICAL ANALYSIS

Differences between groups were compared with unpaired two-tailed *Student's t test* using Prism 7.0 (GraphPad Software, San Diego, CA). A two-tailed paired *Student's t test* and a Two-Way ANOVA analyses with Bonferroni correction made when appropriate and p values indicated on figures. All experiments are representative of at least three independent experiments, unless otherwise noted.

Cell Reports, Volume *36*

Supplemental information

Mds1^{CreERT2}, an inducible Cre allele specific to adult-repopulating hematopoietic stem cells

Yi Zhang, Kathleen E. McGrath, Edward Ayoub, Paul D. Kingsley, Hongbo Yu, Kate Fegan, Kelly A. McGlynn, Sarah Rudzinskas, James Palis, and Archibald S. Perkins

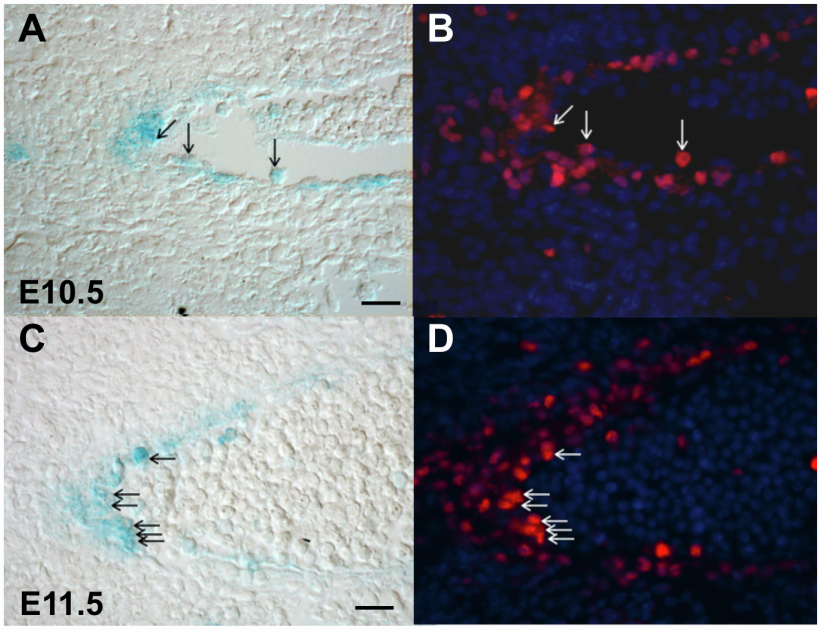

Supplemental Figure 1. *Mds1*^{lacz} labeling and *Runx1* immunohistochemistry relating to Figure 1H.
A-D. Photomicrograph of E10.5 (A, B) or E11.5 (C, D) aorta, left is ventral. β-galactosidase-positive cells (A, C) that also express Runx1 detected by immunocytochemistry (B, D) are indicated by arrows. Size Bars= 20um

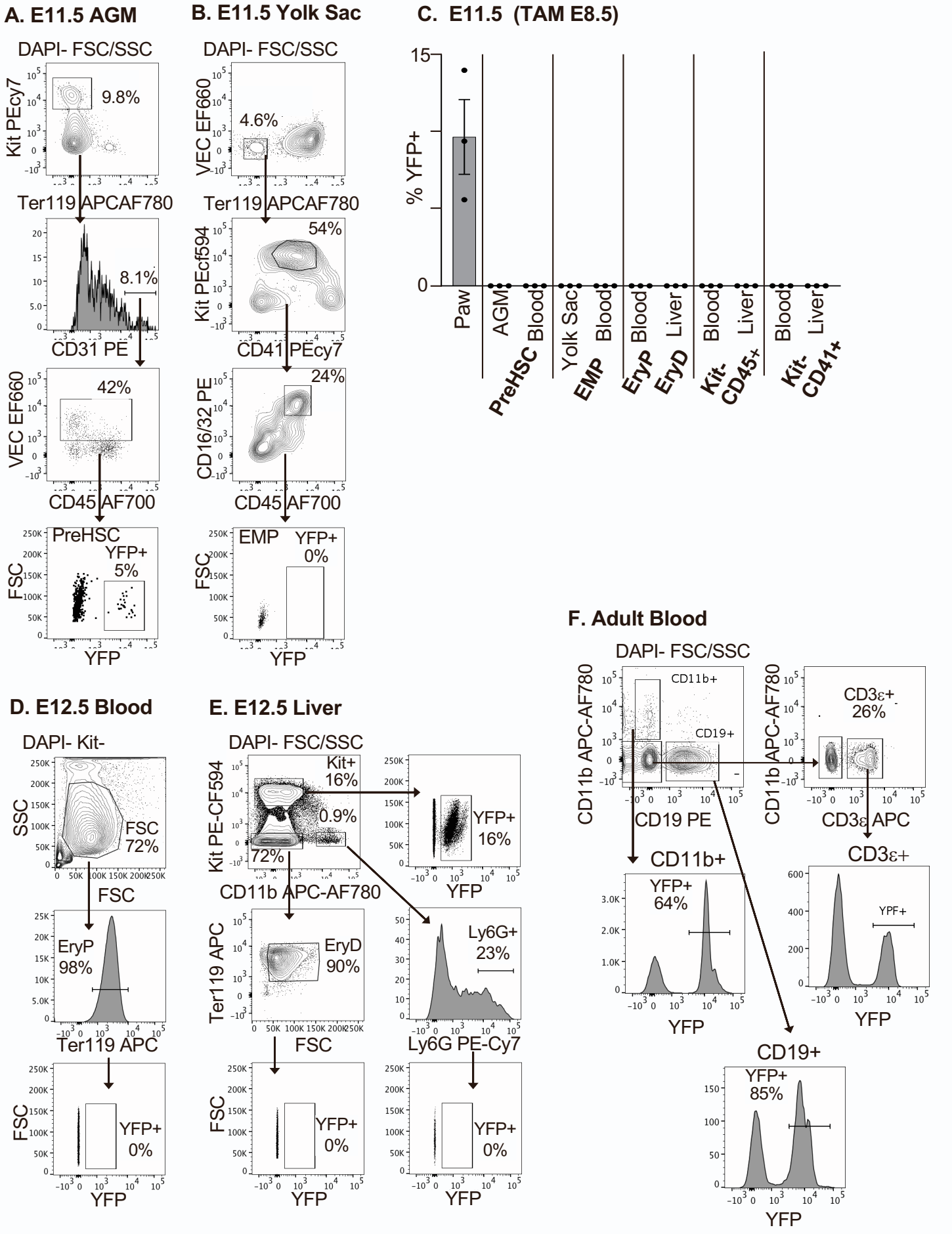
A. E11.5 AGM
DAPI- FSC/SSC
Kit PEcy7
9.8%
Ter119 APCAF780
8.1%
CD31 PE
VEC EF660
42%
CD45 AF700
PreHSC
YFP+
5%
FSC
YFP
B. E11.5 Yolk Sac
DAPI- FSC/SSC
VEC EF660
4.6%
Ter119 APCAF780
Kit PEcf594
54%
CD41 PEcy7
CD16/32 PE
24%
CD45 AF700
EMP
YFP+
0%
FSC
YFP
C. E11.5 (TAM E8.5)
% YFP+
15
0
Paw
AGM
Blood
PreHSC
Yolk Sac
Blood
EMP
Blood
EryP
Liver
EryD
Blood
Kit-
CD45+
Liver
Blood
Kit-
CD41+
Liver
D. E12.5 Blood
DAPI- Kit-
SSC
FSC
72%
FSC
EryP
98%
Ter119 APC
FSC
YFP+
0%
YFP
E. E12.5 Liver
DAPI- FSC/SSC
Kit PE-CF594
Kit+
16%
0.9%
72%
YFP+
16%
YFP
CD11b APC-AF780
Ter119 APC
EryD
90%
FSC
YFP+
0%
YFP
Ly6G+
23%
Ly6G PE-Cy7
YFP+
0%
YFP
F. Adult Blood
DAPI- FSC/SSC
CD11b APC-AF780
CD11b+
CD19+
CD19 PE
CD3ε+
26%
CD3ε APC
CD11b+
YFP+
64%
YFP
CD3ε+
YPF+
YFP
CD19+
YFP+
85%
YFP

Supplemental Figure 2. Gating strategies and support data for Figure 2. **A.** Gating strategy for E11.5 AGM and circulating pre-HSC. Live (DAPI$^-$), FSC/SSC gated cells were further gated Kit+ Ter119-, then CD31+ (PECAM), and finally gated as VEcadherin+ (VEC) with CD45 used to help visualize the populations. **B.** Gating strategy for EMP in the yolk sac or bloodstream. Live (DAPI$^-$), FSC/SSC gated cells were further gated as Ter119- VEcadherin- (to exclude circulating pre-HSC). Then Kit+ CD41^{mid} cells were further gated as CD16/32+. CD45 was used to help further visualize the EMP population. **C.** Analysis of E11.5 *Mds1*^{CreERT2} *Rosa26*$^{LSL\text{-}YFP}$ fetuses after TAM delivery at E8.5. Analyses were performed as in Figures 2H,I, with YFP+ cells in the paws serving as a positive control for *Mds1*^{CreERT2} expression in these fetuses. Average ±SEM of 3 individuals are plotted. **D.** Gating strategy for cells in fetal blood quantitated in Figure 2I, J and below panel E. Primitive erythroid cells (EryP) are gated out of Kit$^-$ Live (DAPI$^-$) blood as Ter119$^+$. **E.** Gating strategy for fetal liver quantitated in Figure 2I, J and below panel E. Live (DAPI$^-$), FSC/SSC gated cells were further gated as Kit$^+$, CD11b$^+$, Kit-CD11b$^-$. CD11b$^+$ were further gated as GR1+, and Kit-CD11b- that are gated by Ter119+ and FSC to gate maturing definitive erythroblasts (EryD). YFP gating demonstrates positivity found Kit+ cell, but not EryD or GR1+ populations. **F**. After RBC lysis, adult peripheral blood cells were initially gated by live (DAPI-) FSC/SSC then gated as CD11b+ myeloid cells, CD19+ B-cells and from the double negative CD3e+ T-cells. Then each population was gated for YFP+.

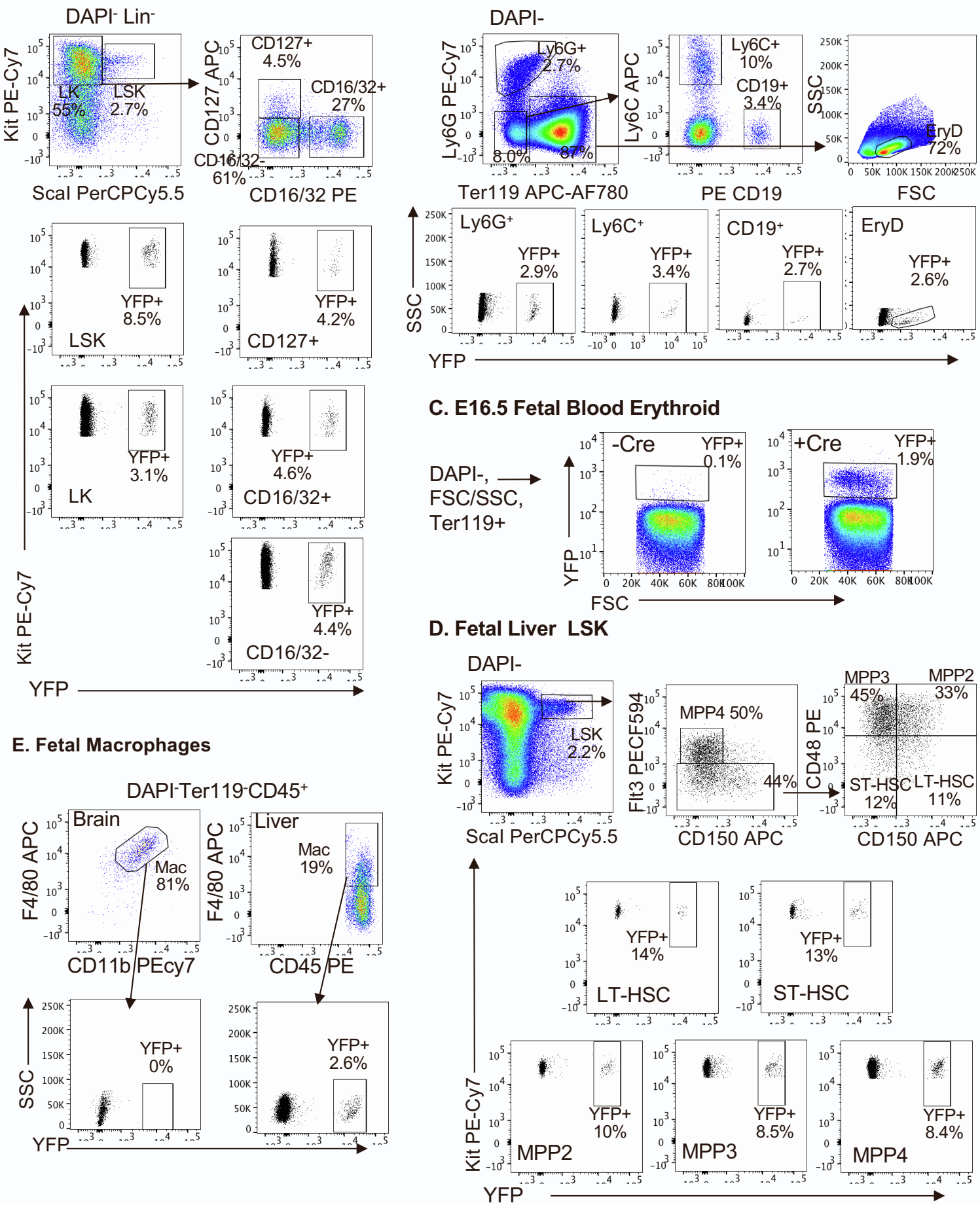
A. Fetal Liver Progenitors
DAPI- Lin-
Kit PE-Cy7
LK- 55%
LSK 2.7%
Sca1 PerCPCy5.5
CD127 APC
CD127+ 4.5%
CD16/32+ 27%
CD16/32- 61%
CD16/32 PE
YFP+ 8.5%
LSK
YFP+ 4.2%
CD127+
YFP+ 3.1%
LK
YFP+ 4.6%
CD16/32+
YFP+ 4.4%
CD16/32-
Kit PE-Cy7
YFP
B. Fetal Liver Lineage
DAPI-
Ly6G PE-Cy7
Ly6G+ 2.7%
8.0%
87%
Ly6C APC
Ly6C+ 10%
CD19+ 3.4%
SSC
EryD 72%
Ter119 APC-AF780
PE CD19
FSC
Ly6G+
YFP+ 2.9%
Ly6C+
YFP+ 3.4%
CD19+
YFP+ 2.7%
EryD
YFP+ 2.6%
SSC
YFP
C. E16.5 Fetal Blood Erythroid
DAPI-, FSC/SSC, Ter119+
-Cre
YFP+ 0.1%
+Cre
YFP+ 1.9%
YFP
FSC
D. Fetal Liver LSK
DAPI-
Kit PE-Cy7
LSK 2.2%
Sca1 PerCPCy5.5
Flt3 PECF594
MPP4 50%
44%
CD150 APC
CD48 PE
MPP3 45%
MPP2 33%
ST-HSC 12%
LT-HSC 11%
CD150 APC
YFP+ 14%
LT-HSC
YFP+ 13%
ST-HSC
Kit PE-Cy7
YFP+ 10%
MPP2
YFP+ 8.5%
MPP3
YFP+ 8.4%
MPP4
YFP
E. Fetal Macrophages
DAPI-Ter119-CD45+
Brain
F4/80 APC
Mac 81%
CD11b PEcy7
Liver
Mac 19%
CD45 PE
SSC
YFP+ 0%
YFP+ 2.6%
YFP

Supplemental Figure 3. Gating strategies utilized in Figure 3. **A.** Example of gating for Figure 3A, B and C. Fetal liver cells were gated to assay YFP positivity of progenitors starting with FSC/SSC, lineage (Ter119, GR-1, CD19, CD3e) negative, live ($DAPI^-$) cells that were then gated as Kit^+ $Sca1^-$ (LK) or Kit^+ Sca^+ (LSK). LK were further gated as CD127+ (CD127+), and then Kit+ CD127- cells were further gated into CD16/32+ and - populations. **B.** Maturing lineages within the fetal liver or blood were gated from a population of FSC/SSC live (DAPI-) Kit- cells (middle graph) as Ly6G+ or Ter119+ or double negative cells. In the liver, Ter119+ cells were further refined for high SSC/FSC (right) to gate erythroblast versus circulating erythrocytes (See C for gating of blood erythrocytes). The double negative cells were future discriminated (left) into CD19+ or Ly6C+ cells. Note that this gating strategy removes the lower Ly6C+ granulocytes (Ly6G+) allowing gating of the Ly6C+ monocytes. **C.** Gating of circulating erythrocytes. Due to the decreasing Rosa expression in erythroid cells as they mature (note the already lower value of liver erythroblasts versus other precursors) the gating of low YFP positivity in erythrocytes above Cre-negative littermates is shown. **D.** Example of subgating of E16.5 LSK quantitated in Figure 3C. LSK were further refined into MPP4- CD135 (Flt3+, CD150-) or LT-HSC, ST-HSC, MPP2 and MPP3 out of the LSK Flt3- cells. **E.** Macrophages were identified by their F4/80 positivity in different tissues from FSC, SSC, live (DAPI-), Ter119- cells. In brain and liver additional CD11b positivity was used but not in fetal liver, which is highly erythropoietic as the macrophages associated with erythropoiesis do not express CD11b (Seu et al., 2017).

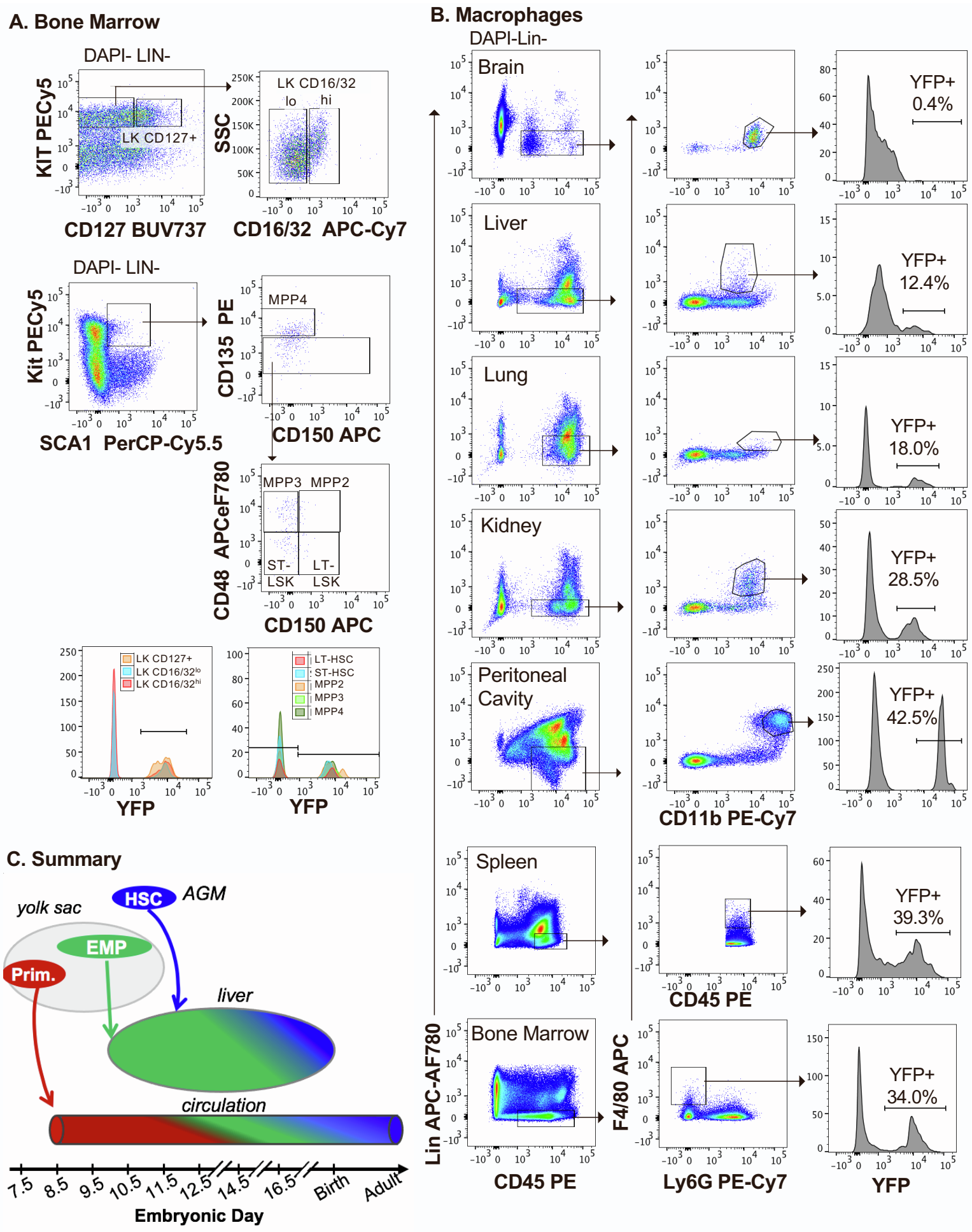
A. Bone Marrow
DAPI- LIN-
KIT PECy5
LK CD127+
CD127 BUV737
SSC
LK CD16/32
lo
hi
CD16/32 APC-Cy7
DAPI- LIN-
Kit PECy5
SCA1 PerCP-Cy5.5
CD135 PE
MPP4
CD150 APC
CD48 APCeF780
MPP3
MPP2
ST-
LSK
LT-
LSK
CD150 APC
LK CD127+
LK CD16/32lo
LK CD16/32hi
YFP
LT-HSC
ST-HSC
MPP2
MPP3
MPP4
YFP
B. Macrophages
DAPI-Lin-
Brain
YFP+
0.4%
Liver
YFP+
12.4%
Lung
YFP+
18.0%
Kidney
YFP+
28.5%
Peritoneal
Cavity
YFP+
42.5%
CD11b PE-Cy7
Spleen
YFP+
39.3%
CD45 PE
Bone Marrow
YFP+
34.0%
Lin APC-AF780
CD45 PE
F4/80 APC
Ly6G PE-Cy7
YFP
C. Summary
yolk sac
HSC
AGM
EMP
Prim.
liver
circulation
7.5
8.5
9.5
10.5
11.5
12.5
14.5
16.5
Birth
Adult
Embryonic Day

Supplemental Figure 4 Gating strategies utilized in Figure 4 and Summary. **A.** YFP positivity of more specified hematopoietic progenitors (top) in adult bone marrow was determine by first gating FSC/SSC, lineage (Ter119, GR-1, CD19, CD3e) negative, live (DAPI-) cells that were then gated as kit+ CD127+ (LK CD127+) and then kit+ CD127- further gated into CD16/32 hi and negative. More multipotent progenitors were gated first (middle) out of the Kit+ Sca+ population (LKS) and further refined into MPP4- CD135 (Flt3+, CD150-) or LT-HSC, ST-HSC, MPP2 and MPP3 out of the LSK Flt3- cells. YFP gating of all populations are shown below. **B.** Macrophages were identified by their F4/80 positivity in different tissues from FSC, SSC, live (DAPI-), lineage (Ter119, CD19, CD19, CD3e) negative cells. For most tissues, additional CD11b positivity was used but not in spleen and bone marrow because of evidence that CD11b- macrophages are involved in erythropoiesis in those tissues (Seu et al., 2017). **C.** Overlapping temporal waves of primitive hematopoietic progenitors and erythro-myeloid progenitors (EMPs) emerge in the yolk sac, followed by hematopoietic stem cells (HSCs), which emerge in the aorta-gonad-mesonephros region (AGM). Differentiated progeny of the primitive hematopoietic lineages enter the newly forming bloodstream beginning at E8.25. EMPs, and then the HSCs, colonize the fetal liver, where they differentiate to produce hematopoietic cells that also enter the circulation. Lineage tracing with Mds1Cre^{ERT2} induced at E9.5 with TAM labels HSC (blue), but not primitive hematopoiesis (Prim. red) or EMP (green) and demonstrates that HSC-derived hematopoiesis increases over time in the fetal liver and in the circulation.